8-23-2021

Design of an Inexpensive PVC Shock Tube for Educational Use

Brandon Edward Bergmann
Rowan University

DESIGN OF AN INEXPENSIVE PVC SHOCK TUBE FOR EDUCATIONAL USE

by

Brandon E. Bergmann

A Thesis

Submitted to the
Department of Mechanical Engineering
In partial fulfillment of the requirement
For the degree of
Master of Science in Mechanical Engineering
at
Rowan University
August, 2021

Thesis Chair: Francis Haas, Ph.D.

Committee Members:
Wei Xue, Ph.D.
Ratan Jha, Ph.D.

Dedication

I would like to dedicate this manuscript to my father, Edward R. Bergmann, Jr.

Acknowledgements

I would sincerely like to acknowledge my advisor, Dr. Francis Haas, for an outstanding investment and dedication towards this project. I would not have had the success in this project if it were not for his care, intellect, and intuition during my time in research. I would also like to thank Rowan University for the privilege of being one of their master's students. I thank Chuck Linderman, Karl Dyer, and Mario Leone for their help with machine operation, guidance, and equipment. I also thank my family and friends for encouragement and prayers through the couple years it took to finish this project. I also thank God for His ever-present guidance, love, and care bringing me to where I am now.

Abstract

Brandon E. Bergmann
DESIGN OF AN INEXPENSIVE PVC SHOCK TUBE FOR EDUCATIONAL USE
2020-2021
Francis Haas, Ph.D.
Master of Science in Mechanical Engineering

Herein is described the design and function of a low-cost, easy-to-assemble, -operate, and -disassemble shock tube platform experiment that can generate shock waves approaching Mach 2 at maximum pressures of ~100 psig with a helium driver gas. The experiment uses several inexpensive (<$5), unamplified piezoelectric sensors attached to a multichannel oscilloscope to monitor the passage of key features of the flow (i.e., incident shock and reflected shock) through the tube, constructed from inexpensive and easy to work with schedule 40 PVC pipe and fittings. From the fixed sensor displacements along the tube and relative differences in respective transit times, the velocities of these flow features can be determined. This permits (1) comparison of experimental results to the theoretical predictions of 1-D transient gas dynamics and (2) a leaping off point for discussion and quantification of non-idealities in the flow, including the shock wave development length, shock attenuation and boundary layer growth, and interactions of the reflected shock and contact surface. Experimental accessories (future work) for study of shock focusing and steady 2-D high speed flows are also briefly discussed. Assuming both pressurized, conditioned air at ~80-100 psig and a modern multi-channel oscilloscope are available at most institutions, the total cost to construct this experiment is around $500.

Table of Contents

Table of Contents (Continued)

Table of Contents (Continued)

List of Figures

List of Figures (Continued)

Figure Page

List of Figures (Continued)

Figure Page

List of Tables

Table Page

Chapter 1

Introduction

Shock tubes are devices used to generate high speed gas flow scenarios. In such scenarios, it is comparatively easy to measure properties of the flow because the gas moves in essentially one dimension, with only slightly more complexity introduced for certain two-dimensional flow configurations (i.e., flow around a wedge). Shock tube facilities are scattered globally, and are used to analyze various situations and experiments encompassing 1-D flow for observing the schlieren effect[1] to testing chemical compounds such as fuel, to understand combustion kinetics or mixing at sudden high pressures and temperatures.[2] Many institutions, such as the National Defense Academy (of Japan);[3] Stanford University,[4] NUI-Galway, Texas A&M, Rensselaer Polytechnic Institute, King Abdullah University of Science and Technology;[5] and NASA[6] have shock tube facilities; however, having a readily-available, inexpensive-to-operate device to physically demonstrate aspects of gas dynamics, such as supersonic gas speeds achievable in the shock tube, can aid educational institutions in teaching compressible flow concepts through a hands-on platform to reinforce and extend the essential theory, which is the primary motivation of this thesis work.

Applications of high-speed flows are numerous, and extend the scope of high-speed flow beyond just aeronautics to inform the design and study of a diversity subjects, including earth reentry capsules,[7] shock wave lithotripsy of gall stones,[8] high temperature chemistry,[1-5] aircraft wing performance,[9] diesel engine fuel injectors,[10] responses of materials to high velocity impacts or intense pulses,[11] sintering,[12] drug delivery,[13] resistive switching in memristors,[14] and wave disk engines,[15] among others. Accordingly, tools that

can facilitate learning of compressible flow and related topics can provide a foundation for seemingly unrelated topics across technological disciplines. Developing an inexpensive shock tube will allow institutions to instruct their students in the basic principles of these wide-ranging applications.

Shock tubes create simplified high-speed flow scenarios. It is comparatively easy to take meaningful measurements of the flow because gas principally moves in one dimension, with slight two-dimensional flow if applicable (i.e., flow around a wedge). Generally, a shock tube is separated by a diaphragm into two parts, a high pressure (driver) and low pressure (driven) section. When the diaphragm is broken, the high-pressure gas contained in the driver section creates pressure waves that propagate into the low pressure (driven) section. These waves develop into pressure front that moves faster than the speed of sound in the low-pressure gas (a shock wave). When this occurs and the shock front passes by sensors mounted in the driven section of the shock tube, these sensors can readily detect the disturbance signal. Knowing the distance between sensors and the time it took the shock wave to pass between sensors permits computation of a shock wave velocity, which is an application of the time-of-flight (ToF) principle. Additional complexities in the flow arise but having a readily available device to physically demonstrate ToF aspects of gas dynamics can give institutions a better mechanism for teaching at a hands-on perspective for students learning one- and two-dimensional high-speed flow.

Again, the shock tube addressed in this thesis is being designed to be of low cost, enabling institutions to be able to construct it (or a variant) for no more than a few hundred dollars. The shock tube will be built for ease of accessibility. This will include use of the institution's own utilities and facilities such as gas, experimental space, and storage. This

facility assumes that the uses will have access to a measuring and recording device, such as an oscilloscope, for viewing the recorded disturbances in the sensors due to the passage of the pressure waves. These particular objectives/constraints/assumptions differentiate this work from many existing shock tube facilities that have been purpose-built for a variety of reasons, some of which have been previously cited. Though many institutions have shock tube facilities, these are often used nearly exclusively for research. Many more institutions are without a shock tube, presumably due to the high cost of developing a facility, the space needed for such a facility, or both. The present objective is to develop a tool that will overcome these barriers and give the educational benefit of hands-on learning for one- and two-dimensional gas dynamics.

Chapter 2

Theoretical Basis

Shock Tube Theory

As stated in the introduction, a shock tube is initially divided into two sections: the driver section (higher pressure) and driven section (lower pressure), separated by a diaphragm. When the diaphragm is broken, the driver gas makes its way into the driven section, creating compression waves that eventually (within milliseconds) coalesce into a shock front. According to discussion of Gaydon and Hurle[1], idealized shock wave formation occurs in the following way: consider a long tube that has a piston capable of reaching velocity *v*. If time zero is the instant the piston begins to accelerate from rest to velocity *dv* (i.e., the diaphragm breaks, permitting a driver gas "piston" to accelerate into the driven section), a first small compression wave forms and propagates into the driven gas. This wave moves at the speed of sound *a* in the driven gas. As the piston (driver gas front) continues to accelerate to a new instantaneous velocity 2*dv*, a second compression wave of speed $a + da$ forms in the driven section; the wave speed is higher by *da* since the second wave is propagating in slightly compressed gas from the first compression wave. This second compression wave will ultimately catch the first wave, strengthening the amplitude of compression at the wave front. This process repeats until, after some short time, the piston reaches its maximum velocity *v*, resulting in all compression waves coalescing into one strong compression wave with a velocity W_S. This is called a *shock wave*. The *S* in W_S corresponds to the incident shock wave before it reflects off the shock tube end wall. The reflected shock wave speed discussed later will have the notation W_R.

The shock tube can be analyzed graphically with respect to position and time. An x-t diagram is used to visualize the regions of flow that form just a small time after the diaphragm breaks.

Figure 1

Graphical Representation of a Shock Tube

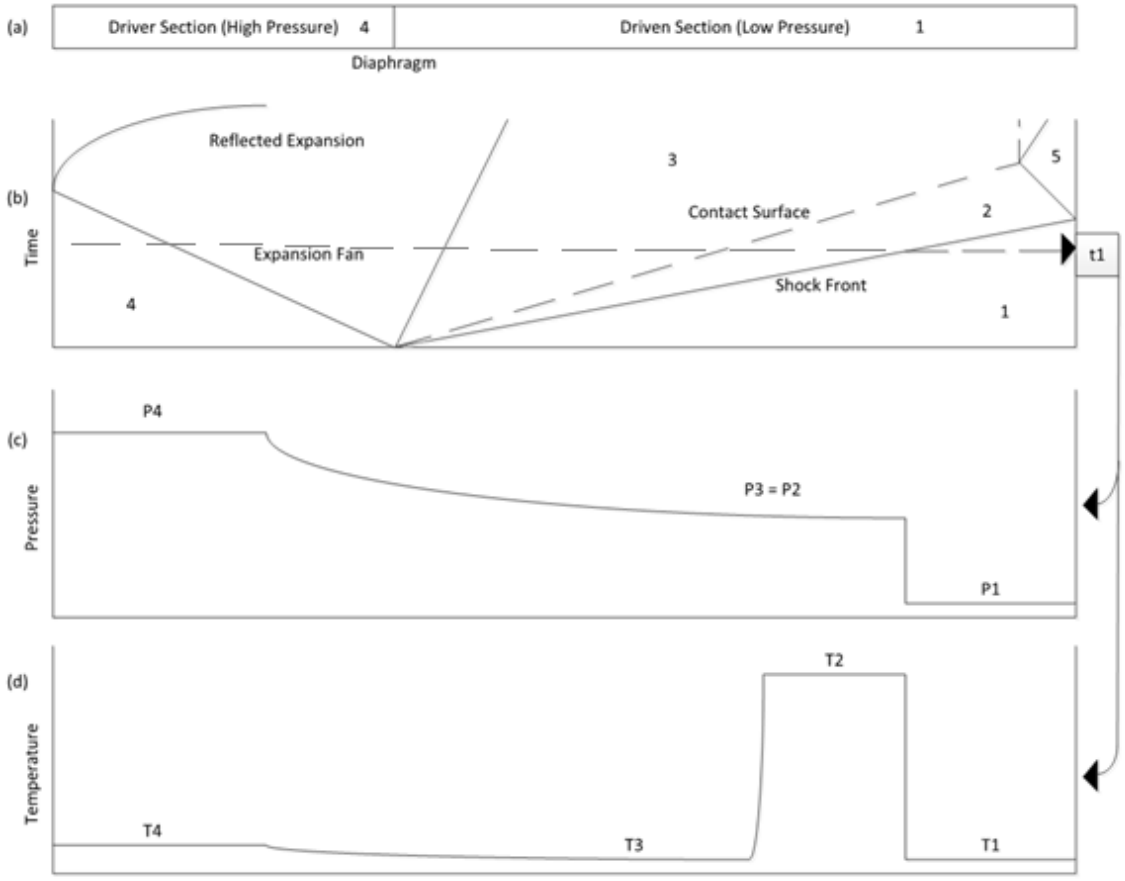

Note. The sections of this figure are: (a) the initial condition before bursting the diaphragm, (b) an x-t diagram for the waves generated from bursting the diaphragm to a time showing the different regions (1-5) discussed in the text, (c) the different pressures at time t_1, and (d) the different temperatures at time t_1. Adapted from Gaydon & Hurle.[1]

Figure 1 a represents the shock tube in its initial states before the diaphragm breaks. The shock tube is separated into the high pressure (driver) and low pressure (driven) gases,

described by thermodynamic states (4) and (1), respectively. Figure 1 b, representing all locations in the shock tube (x-axis) at short times ($t \geq 0$) indicates five different regions, corresponding to different gas conditions. The fourth and first regions indicate the undisturbed driver and driven gases as indicated in Figure 1 a. Region (2) indicates the shock-compressed driven gas that exists between the shock wave front and the front of the driver gas (contact surface). Region (3) indicates the expanding driver gas existing between the contact surface and the rarefaction fan. Region (5) is the doubly compressed gas between the reflected shock front and the end of the tube the shock wave reflects from. Gas in front of the incident shock (Region (1)) has zero velocity since it is undisturbed; however, gas affected by the incident shock is pushed to relatively high velocity due to shock wave compression. When the shock wave hits the end wall of the shock tube, it reflects, stopping the originally induced mass motion of compressed gas to a velocity of zero, at the same time compressing it again.

While the diaphragm is intact, both sections have certain initial pressures and temperatures, with Region (4) as the higher pressure and Region (1) as the lower pressure (temperatures need not be $T_4 > T_1$). Figures 1c and 1d describe, respectively, the spatial pressure and temperature distributions along the shock tube at a representative time t_1 between the diaphragm bursting and the shock front reflecting from the end wall. When the shock front moves into Region (1) it increases the pressure and temperature of the driven gas to P_2 and T_2, while also inducing a mass motion of the gas affected by the shock wave. The contact surface moves at the speed of sound a, and the pressures in Region (2) and where Region (2) contacts Region (3) at the contact surface are equal. On the driver

side, expansion waves propagate in the opposite direction as the incident shock wave, decreasing the pressure and temperature as these waves move toward Region (4).

Ideal Gas Case

This project will be centered around ideal gas physics as the assumption of ideality is appropriate for the gases and conditions used in this project. Another good reason for using ideal gases is a factor of safety. Using some non-ideal gases can be harmful to breathe as the constant opening of the shock tube exposes the gases inside to the environment. Facilities using metal shock tubes are for better use in studying chemical ignition and mixing, so this project will not use explosive gases. To better understand the properties of the shock tube, simple equations can be manipulated in finding the different equations of state for each region.[1] We begin by showing the mass, momentum, and energy equations for flow across a shock wave in the shock-stationary frame of reference; these respective quantities are conserved across the shock wave.

$$\rho_1 u_1 = \rho_2 u_2 \tag{1}$$

$$P_1 + \rho_1 u_1^2 = P_2 + \rho_2 u_2^2 \tag{2}$$

$$H_1 + \frac{1}{2} u_1^2 = H_2 + \frac{1}{2} u_2^2 \tag{3}$$

where ρ is the density, u is the relative velocity, P is the absolute pressure, and H is the specific enthalpy of unit mass. Along with the ideal gas equation of state, these equations can be substituted into each other to provide the enthalpy equation

$$H = E + RT = \left(\frac{\gamma}{\gamma - 1}\right) RT \tag{4}$$

where E is the specific internal energy, R is the specific gas constant, T is the absolute temperature, and γ is the specific heat ratio. We also know that the definition of Mach number for the shock front is

$$M_1 = \frac{u_1}{a_1} = \frac{W_s}{a_1}. \tag{5}$$

We can rearrange and substitute the equations above to find the ratio of the pressures, densities, and temperatures of regions 1 and 2, which are

$$\frac{P_2}{P_1} = \frac{2\gamma M_1^2 - (\gamma - 1)}{\gamma + 1} \tag{6}$$

$$\frac{\rho_2}{\rho_1} = \frac{(\gamma + 1)M_1^2}{(\gamma - 1)M_1^2 + 2} \tag{7}$$

$$\frac{T_2}{T_1} = \frac{\left(\gamma M_1^2 - \frac{\gamma - 1}{2}\right)\left(\frac{\gamma - 1}{2}M_1^2 + 1\right)}{\left(\frac{\gamma + 1}{2}\right)^2 M_1^2}, \tag{8}$$

where $\gamma = \gamma_1$.

Moving onto the expansion fan, the two ends of the fan are moving with an isentropic expansion, for which the expression

$$\frac{2a}{\gamma - 1} + v \tag{9}$$

is conserved. Here v is the actual velocity of the wave, and a is the speed of sound in the gas. Through the conservation equation, by setting both sides of the equation to the values of regions 3 and 4, knowing that the gas in region 4 is undisturbed having a zero velocity develops the equation

$$\frac{2a_4}{\gamma_4-1} = \frac{2a_3}{\gamma_3-1} + v_3. \tag{10}$$

Knowing that the velocities and pressures on both sides of the contact surface are equal, $v_3$is replaced by v_2.For the adiabatic expansion process

$$\frac{P_4}{P_3} = \frac{P_4}{P_2} = \left(\frac{a_4}{a_3}\right)^{\frac{2\gamma_4}{\gamma_4-1}} \tag{11}$$

and combining equations 10 and 11,

$$\frac{P_4}{P_2} = \left(\frac{a_4}{a_4 - \frac{\gamma_4-1}{2}v_2}\right)^{\frac{2\gamma_4}{\gamma_4-1}}. \tag{12}$$

Substituting equations for $\frac{P_2}{P_1}$ and $\frac{P_4}{P_2}$

$$\frac{P_4}{P_1} = \frac{2\gamma_1 M_1^2 - (\gamma_1 - 1)}{\gamma_1 + 1}\left\{1 - \frac{\gamma_4-1}{\gamma_1+1}\frac{a_1}{a_4}\left(M_1 - \frac{1}{M_1}\right)\right\}^{-\left(\frac{2\gamma_4}{\gamma_4-1}\right)}. \tag{13}$$

Equation 13 is particularly relevant for this study as it permits prediction of the incident shock wave velocity (through M_1) as an algebraic function of gas conditions in the driver gas (4) and driven gas (1) prior to diaphragm burst. In particular, $M_1 = fn(P_4, T_4, \gamma_4, MW_4, P_1, T_1, \gamma_1,$ and $MW_1)$, where MW indicates the average molecular weight of the gas, which influences the sound speed, *a*.

In finding the velocity of the contact surface, which is the velocity of the region behind the incident shock front, v_2, the equations used from the incident shock

$$u_1 = W_s - v_1 \tag{14}$$

$$u_2 = W_s - v_2 \tag{15}$$

$$\rho_1 u_1 = \rho_2 u_2 \tag{16}$$

$$\frac{\rho_2}{\rho_1} = \frac{(\gamma + 1)M_1^2}{(\gamma - 1)M_1^2 + 2} \tag{17}$$

can be substituted into each other to produce

$$v_2 = \frac{2a_1}{\gamma + 1}\left(M_1 - \frac{1}{M_1}\right). \tag{18}$$

With the analogy considering the gas being at rest before the diaphragm bursts, $v_1 = v_5 = 0$, the above equation can be written as

$$v_2 = \frac{2a_2}{\gamma+1}\left(M_R - \frac{1}{M_R}\right), \tag{19}$$

where

$$M_R = \frac{u_2'}{a_2} = \frac{W_R + v_2}{a_2}. \tag{20}$$

Using the relationship

$$\left(\frac{a_2}{a_1}\right)^2 = \frac{P_2}{P_1}\frac{\rho_1}{\rho_2} \tag{21}$$

we can use the previous equations to form the equation

$$\frac{P_5}{P_2} = \frac{\frac{\gamma + 1}{\gamma - 1} + 2 - \frac{P_1}{P_2}}{1 + \frac{\gamma + 1}{\gamma - 1}\frac{P_1}{P_2}}. \tag{22}$$

Using the ideal gas law, the temperature ratio is

$$\frac{T_5}{T_2} = \frac{P_5}{P_2}\left\{\frac{\frac{\gamma+1}{\gamma-1}+\frac{P_5}{P_2}}{1+\frac{\gamma+1}{\gamma-1}\frac{P_5}{P_2}}\right\}. \tag{23}$$

Substituting the equations for regions 1 and 2 and the ones above will lead us with equations comparing the reflected values to region 1 from initial conditions giving us

$$\frac{P_5}{P_1} = \left\{\frac{2\gamma M_1^2-(\gamma-1)}{\gamma+1}\right\}\left\{\frac{(3\gamma-1)M_1^2-2(\gamma-1)}{(\gamma-1)M_1^2+2}\right\} \tag{24}$$

$$\frac{T_5}{T_1} = \frac{\left\{2(\gamma-1)M_1^2+(3-\gamma)\right\}\left\{(3\gamma-1)M_1^2-2(\gamma-1)\right\}}{(\gamma+1)^2M_1^2}. \tag{25}$$

In similar fashion to Equation 13, both Equations 24 and 25 permit prediction of key flow parameters based only on initial conditions of the gases contained within the shock tube.

Using these equations, we were able to make a spreadsheet to predict key incident and reflected shock parameters and compare to results from Gaydon and Hurle[1] with success. The only problem encountered was in determining the relationship between reflected shock wave velocity and reflected shock Mach number. Though the equation from Gaydon and Hurle[1] was used, the values did not match up to what was expected, so a different approach was needed to find the correct equation.

Reflected Shock Verification

Anderson's compressible flow text[16] provides an alternative means of relating the reflected shock velocity and its Mach number using the relation of the Mach numbers of the incident M_S and reflected M_R shock wave fronts of a calorically perfect gas:

$$\frac{M_R}{M_R^2-1} = \frac{M_S}{M_S^2-1}\sqrt{1+\frac{2(\gamma-1)}{(\gamma+1)^2}\left(M_S^2-1\right)\left(\gamma+\frac{1}{M_S^2}\right)}. \tag{26}$$

This cannot be solved explicitly, so an algebraic form is needed to find the reflected Mach number. Having this, we can then solve for the velocity of the reflected shock wave directly. Also, in this form there is a limiting case. As the limit of both sides of this equation go to the weak shock wave limit $\lim_{M_R \to 1}$ (i.e., a sound wave), the limit does not exist because of division $\lim_{M_R \to 1}$, the equation equals zero. To simplify the algebra, the right side of the equation can be made into a simplifying function $q = q(M_S)$ after taking the inverse of both sides, so

$$\frac{M_R^2 - 1}{M_R} = q(M_S). \tag{27}$$

Putting this in a quadratic formula and solving for M_R,

$$0 = M_R^2 - q(M_S)M_R - 1. \tag{28}$$

$$M_R = \frac{q(M_S) \pm \sqrt{\left(q(M_S)\right)^2 + 4}}{2}. \tag{29}$$

The physically relevant solution is the root based on addition in the numerator appearing in Equation 29. Once M_R is found W_R can be found through relations from Gaydon and Hurle[1]. The Mach number of the reflected shock wave is defined as

$$M_R = \frac{u'_2}{a_2}, \tag{30}$$

where $u'_2 = W_R + v_2$.

Solving for W_R,

$$W_R = a_2 M_R - v_2. \tag{31}$$

The results of the ratio of the reflected to the incident shock speed were compared with the values in Table II.3 in Gaydon and Hurle and proved to be very similar, keeping in mind that Gaydon and Hurle's book was published in 1963 and may include rounding differences.

Shock Wave Development Length

Now that key observables for the ideal gas dynamic case have been solved, different ideal gases can be tested at different experimental scenarios to compare measured behavior compared to what is predicted by one-dimensional theory. Permanent gases that can be used for the pedagogical purposes describe here besides air (or nitrogen) include argon, carbon dioxide, and helium. Argon and carbon dioxide are heavier and at otherwise comparable initial conditions, provide a slower incident shock velocity than air, but helium is lighter (MW_{He} = 4 g/mol vs. MW_{air} = 29 g/mol) and provides much greater shock velocity.

Since the essential theory has been described, design and data acquisition are nearly ready to be determined. But first, the shock wave development length must be determined first to know how much minimum length is needed for the shock to develop in the driven side. This permits thoughtful placement of the shock wave sensors at the right place. Figure 2 shows how the shock wave develops in time while the contact surface, or "piston", accelerates to the ideal velocity indicated in Figure 1. Between the shock development line and piston path, there are lines that intersect them that can be used to find the length needed for the shock wave to develop by using algebraic terms. As the "piston" uniformly accelerates from rest in the tube, skipping the derivation, the equation to calculate the shock wave development length is seen in Equation 32,

$$x_{shock} = \frac{2c_0^2}{(\gamma - 1)a}, \tag{32}$$

as seen in.[17] To get an estimate for the acceleration of the shock wave, a given acceleration $a = 4 \cdot 10^4 m/s^2$ was taken from a problem for finding shock wave development length was taken[18]. At 300 K the speed of sound in air $c_0 = 346.92\ m/s$, and gamma for air is 1.4. Substituting these values into Equation 32 gives a development length of 2.507 m or 8.2 ft. This method of using a textbook problem may sound absurd, but the shock wave development length found can be compared to Gaydon and Hurle[1] where they quoted formation distance in a 3¼ inch square tube from White,[19] who tested diaphragm opening times with hydrogen as the driver and argon as the driven gas. The graph showed that at a pressure ratio of 368, with a testing bursting pressure range of 15-30 atm, the shock wave was at its greatest strength at roughly twelve feet. As the pressure ratios increased, the formation distance increased. So, 8.2 feet is safe to assume as the greatest pressure ratio allowed for operation in a three-inch schedule 40 PVC pipe is 14 (the maximum operating pressure will be ~220 psi).

Figure 2

Compression Wave Converging to a Shock in the X-T Plane

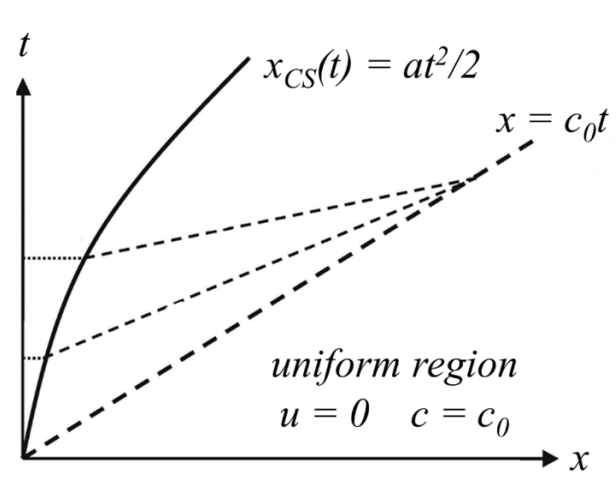

Note. The straight line denotes the shock wave, and the curved line denotes the contact surface. The dotted lines intersecting both lines indicated when the shock wave develops. Figure adapted from Introduction to Simple Shock Waves in Air with Numerical Solutions Using Artificial Viscosity, by Seán Prunty. [17]

Thermodynamic Case

At long times, the gas dynamic cases considered above tend toward equilibrium, from which final thermodynamic states in the shock tube can be determined. For the ideal case, we are assuming that the process is calorically and thermally perfect, meaning the energies are proportional to the absolute temperature of the gases. In this process the only desired information is what the system, the shock tube, will be at time $t = \infty$,which will be effectively achieved a few seconds after the diaphragm breaks. In other words, the details of the gas dynamic process is not of concern. In the initial condition state before the diaphragm breaks, the driver and driven gases are completely thermodynamically characterized by initial pressures, temperatures, heat capacity ratios, and average molecular weights. Along with the geometry of the tube sections, this is sufficient information to

compute other important initial and final gas properties such as speed of sound in the gas, volume of the gas (depends on the inner tube diameter), constant pressure and constant volume specific heats, total moles of gas, specific molar enthalpies, internal energies, as well as entropies, enthalpies, and internal energies of each gas.

Shock Tube Implementation

For the pedagogical objectives of our experiment, we only desire the measurement of only one variable. In the normal mode of operation, out of the eight initial variables including pressure, temperature, gamma, and molecular weight for both the driver and driven gases, the pressure of the driver gas will be varied to compare the measured shock wave velocities to mathematical solutions of the gas dynamic case (i.e., via Equations 13 and 26).

Because the equations are implicit, it was difficult to solve mathematically for the Mach number in terms of initial pressure ratios, so it is used as the independent variable in a spreadsheet used to get compute the desired pressure for the driver gas in experiments. The values computed were verified with table II.3 in Gaydon and Hurle.[1] With a university using compressed air lines regulated to 100 psia (~6.9 bar), which is reasonable for many universities and also accessible by small utility compressors, and the driven gas at absolute atmospheric pressure and room temperature, the shock wave can reach a Mach number of 1.453. This means the shock tube should be able to record supersonic velocities.

Chapter 3

Theoretical Design

Shock Tube Parameters

Having established some essential shock tube theory in the preceding chapter, this chapter focuses on design of the shock tube to be implemented in this study. Shock tube designs used at different institutions were surveyed to representative dimensions of existing shock tubes. Shock tubes for different applications, such as high pressure, low pressure, chemical, etc., were gathered and compared to help set an average length and diameter of the shock tube to be constructed at Rowan University. Parameters for the different shock tubes were organized into a plot (Figure 3) that compares the length to diameter ratio (L/D) and driver volume to driven volume (V_4/V_1). Not all studies surveyed indicated all the relevant dimensions, so only the sources that included at least a total length and diameter were used. Every length to diameter ratio was calculated by using the indicated diameter of the driven section. Our shock tube will have the same diameter the whole length of the tube for simplicity of design and pedagogical calculations; however, some shock tube facilities surveys had a large difference in driver to driven diameters, so the driven diameters in these cases were not considered in the calculation for making the whole diameter of the shock tube true to our design. Instead, the driven section was used in these cases to formulate our shock tube.

Figure 3 shows that the driver-to-driven section volume ratios are mostly around 1:3. Our shock tube model will have a diameter of 3 inches for easy access, and many of the shock tubes researched have a driven section diameter of around 3 inches, as seen in Figure 4. The minimum and maximum L/D boundaries are included as a recommendation

of Gaydon and Hurle[1], who state that the length to diameter ratio of the shock tube should be between 40 and 100. Additionally, they suggest a diameter between 1 and 4 inches. Both considerations are among the constraints for our final product.

Figure 3

Sampling of Driver to Driven Section Volume vs. Length to Diameter of Shock Tubes Used at Different Institutions [2 18 20 21 22 23 24 25 26 27 28 29 30 31 32 33]

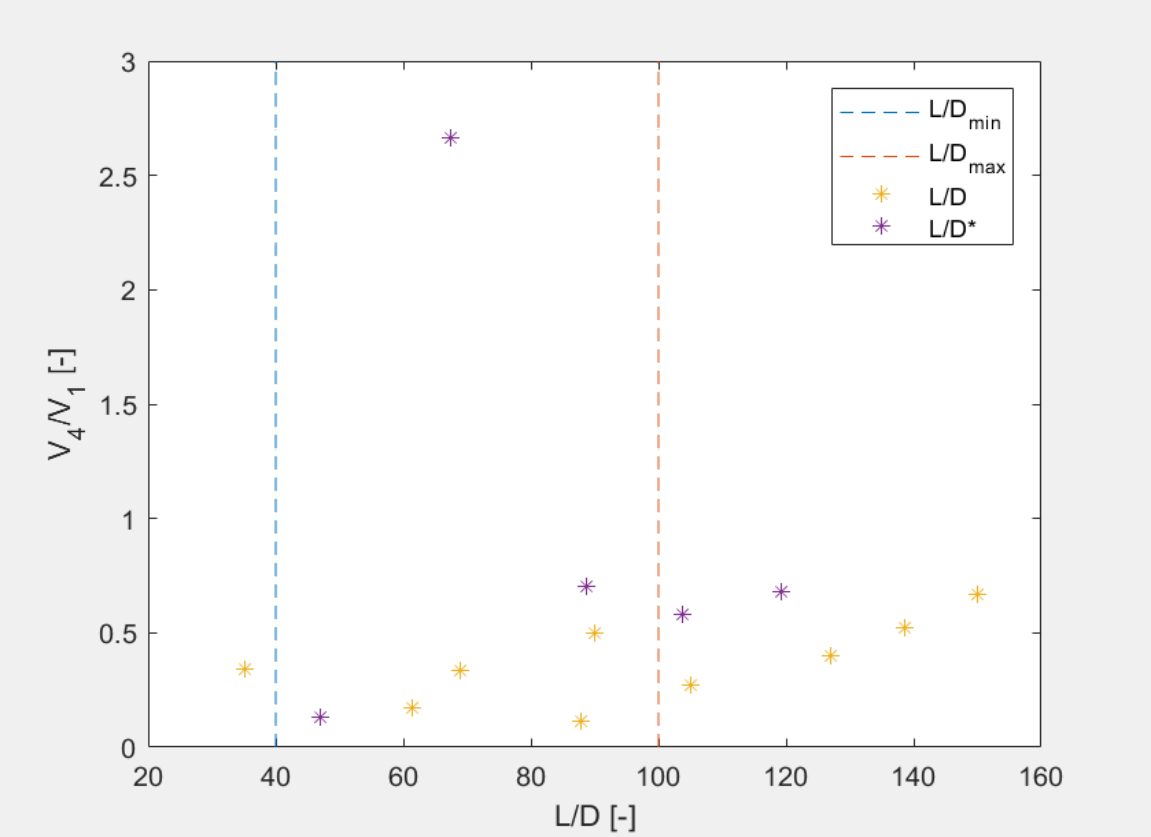

Figure 4 shows that most of the diameters of the driven section were around three inches. This is a plausible diameter not only for considering the shock tube literature review of different institutions' shock tube facilities but also because there are practical reasons for such a diameter. For one, three inches wide enough for easy access and to facilitate

certain modifications, adjustments, and repairs as a normal sized hand and arm should fit inside of a three-inch inner diameter pipe. Another reason is that a standard schedule 40 PVC pipe has a higher-pressure rating in a three-inch pipe than a four-inch pipe.[34] This is a key consideration for constructing a PVC shock tube with pressures greater than 100 psi. Lastly, a three-inch pipe has a wider radius of curvature than a smaller sized pipe, providing a greater convenience to create mounting hardware for stability and sensor placement than a smaller inner diameter pipe.

Figure 4

Sampling of Driven Section Diameter vs. Length to Diameter of Shock Tubes Used at Different Institutions [2 18 20 21 22 23 24 25 26 27 28 29 30 31 32 33]

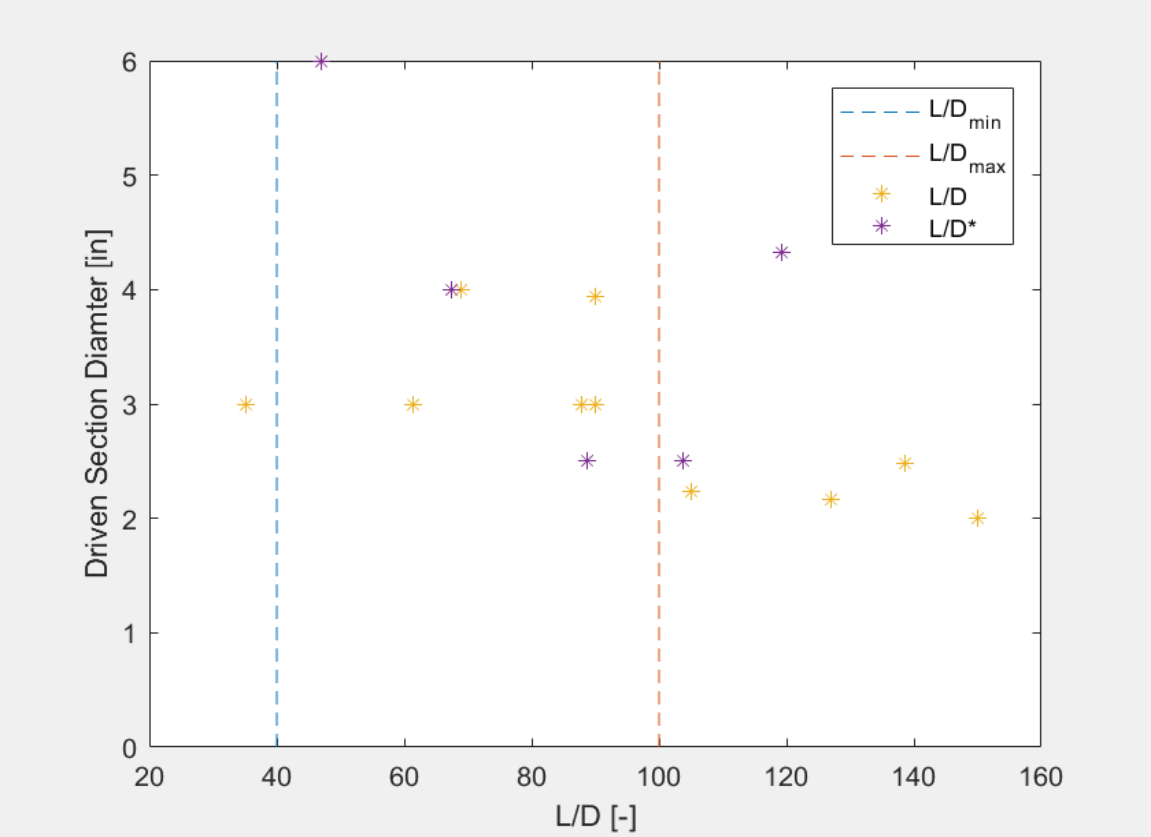

In reviewing the dimensions gathered from the different shock tube facilities, the total length of the shock tubes from most facilities ranged from 20 to 25 feet, with most in this range being 22 to 23 feet and some around 29 feet. With a set diameter of 3" and the recommended L/D between 40 and 100, the minimum and maximum total length of our shock tube can be 10 and 25 feet, which overlaps the range of many of the other shock tubes surveyed here. Considering everything discussed from the dimensions of the shock tube, the diameter, total length, driver section length, and driven section length will be, respectively, three inches, 20 feet, 5 feet, and 15 feet. Length increments of 5 feet simplify construction as PVC pipe is often sold in 10' lengths. This minimizes cutting of pipe and re-joining using flanges. This length will help with spatial considerations.

For the Rowan shock tube to occupy 20 feet in length, additional considerations are warranted. A shock tube can be placed in a classroom or a demonstration lab, which is reasonable in many cases. However, the Rowan shock tube design will be able to fit in a hallway for demonstration since the primary concern for placement and transportability is the total length and disassembled section lengths. To aid in transportation and storage, the shock tube can be divided into four, five-foot sections, permitting it to easily fit inside a relatively small elevator of width 80 inches.[1]

To reduce cost and maximize ease in developing, PVC piping, as stated earlier, will be used to create our shock tube, as stated earlier. As reference, a PVC shock tube has been completed before[11] with a maximum pressure capability of 1.4 MPa (203 psi). However, we limit our interest to PVC pipes that are robust enough to withstand 100 psi (an assumed value for regulated pressure of utility air lines in many academic laboratory buildings), and 3-inch schedule 40 PVC can withstand about double that pressure.[34] 3-inch PVC is

inexpensive, selling at around $20 USD per 10 feet of pipe at many local hardware stores. It is also easier to modify and build with than metal, so if a mistake is made, it can easily be cut or discarded. Weight is also a factor as metal designs will tend to be heavier than PVC.

Sensor Research

Having fixed the dimensions of the shock tube enables determination of shock wave passage sensor locations. More research was performed in determining existing ideas and developing intuition for what sensors can be used. The goal for this project is to achieve simplicity and low cost while maintaining an adequate response time for gathering information of a shock wave passing. It needs to be known when the shock wave has passed a sensor (i.e., time of flight), providing a broad spectrum of sensor types that can be used.

Different ideas for sensing passage of shock waves are discussed in Gaydon and Hurle[1], including pressure transducer detectors, optical detectors (light-schlieren and reflection), temperature-sensitive resistance detectors, positive-ion beam detectors, glow-discharge detectors, and ionization detectors. Some of the ideas use very high voltages which are not readily available at every institution and may pose safety risks. Further, the devices mentioned in the chapter are complicated to make. This book was published in the early 1960's so there weren't cheaper, accessible sensors that could be purchased. Nevertheless, it is instructive to briefly review a diversity of options for shock wave speed measurement.

An LED-photoresistor configuration can detect a shock wave passing by the change in the refractive index of the gas through which the beam passes. This deflects the light beam, decreasing the light intensity the photoresistor receives, resulting in a change in the

signal from the data acquisition system. Similar schlieren sensors can take up valuable laboratory space and be more tedious to build than using an LED light and a photoresistor. Temperature-sensitive resistance detectors must be handmade and heat treated at high temperatures up to 600°C after careful machining; however, such sensors are durable. As far as ionization detectors, a simple design that uses spark plugs is noted. In this, a shock wave can disrupt the flow of ions when passing, causing a disruption in the signal, but this technique requires high voltage.

Today, sensor technology has evolved, and we have the luxury of using less expensive, simpler ideas. Piezoelectric sensors can be bought inexpensively and have a characteristic time fast enough for this project to give an acceptable response for accurate detection of shock wave passage. A high-quality oscilloscope or other data acquisition system requires no amplification, leading to a very simple sensor for time-of-flight measurements. The low price of a few dollars per sensor permits purchase of multiple sensors in case there is any damage caused by mishandling or through experimentation.

For the signal response time, the sensor used needs to be fast enough to pick up a signal moving at the speed of the shock wave or faster. The fastest shock wave anticipated in the present facility is driven by helium at 100 psig (6.9 barg) into air maintained at atmospheric pressure. At these conditions, the incident shock velocity will be 630 m/s. Assuming a sensor will be around 1 cm in length, the response time will have to be at most 15 μs, suggesting that a piezo sensor with a frequency above ~70kHz would be adequate to accurately detect shock passage.

Chapter 4

Build

Sensor Ideas and Choice

The first decision for the build of the shock tube was which sensor would be used. Different premade sensors were researched from various websites on price and response time. Pressure transducers were ruled out since most were priced at least ~$40 USD/each up to a couple or few hundred dollars each. Piezoelectric sensors are inexpensive and can be bought at less than $5 each for most sensors. Note that these are bare sensors with leads attached. Quite a few of these sensors are fast enough to have a response time of less than 15 μs, which makes a good candidate. Two types of photodiodes, ambient light and infrared, were researched. The ambient light photodiode is at a very inexpensive price of $0.45 USD/each with a spectral range of 480 - 560 nm, making it an economical sensor. The response time is 6 μs, but the viewing angle is 120°. Nevertheless, the ambient light photodiode is a good candidate. The infrared photodiode is $0.45 USD/each with a rise and fall time of 100 ns. Having the same shape of an LED bulb, it can easily be inserted into the walls of the shock tube which can decrease the reception angle. The temperature-sensitive resistance detectors have too slow of a response time of less than one second. Light schlieren sensors are not very simple to produce and require more calibration as knife edges are used to occlude part of the light beam. Also, this would require a device to provide power to the sensors. This would ultimately leave the final price of the equipment to be too expensive in considering the goal of the project. Lastly, fiber optic pressure sensors are listed at least $100 USD/each.

Ultimately, the sensor chosen was the piezoelectric sensor. It would need thought in creating a housing to place the sensor on, but it was the simplest sensor to incorporate into the project. The photodiodes would have to notice a change in refraction from the beams to have a change in signal, which before buying the sensors is not guaranteed in a sealed shock tube.

Prototype Shock Tube

The piezoelectric sensor was tested to discover if it would work and transmit a fast-enough response. We tested shots with a Tektronix TDS 360 oscilloscope last calibrated in 1996. The oscilloscope was useful as it had a nominal speed of 200 MHz, which was more than enough for what was required for the sensor signal acquisition time.

The initial "shock tube" apparatus involved a 10-inch-long, 3" nominal diameter schedule 40 PVC pipe with two reducing bushings on either end to for attaching a ball valve connected to a high-pressure line and the driven section, respectively (Figure 5). The ball valve supported a pressure gauge and an overpressure safety valve. Driver and driven sections were separated by a solenoid activated by an electric switch. The driven side was 20 ft of ¾ inch schedule 40 PVC pipe with a piezoelectric sensor on the open end. The sensor was glued to a small 3D printed fixture which gave enough space for the sensor to sit and not block any significant cross-sectional area of the open tube. With some testing, calibration, and oscilloscope manual knowledge, we were able to see spikes in real time after filling the driver section and actuating the solenoid. Seeing responses let us move onto collecting shock wave data with a prototype shock tube, which would be the same shock tube but with a shorter driven section.

Figure 5

Driver Section of the Prototype Shock Tube

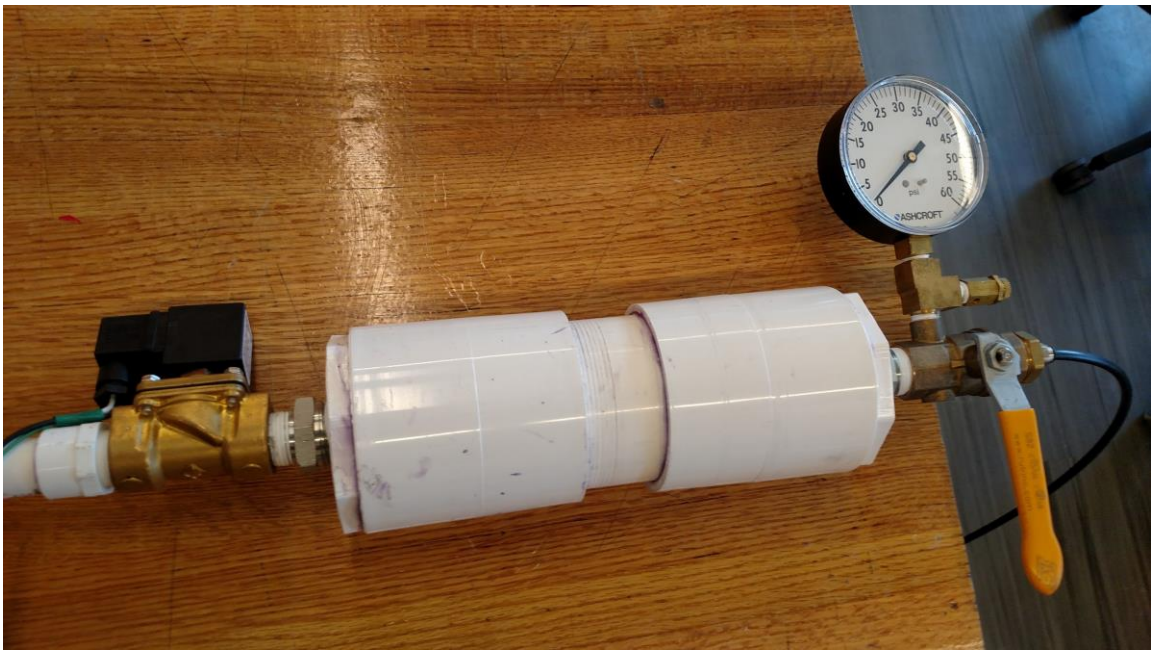

Note. Pressure Gauge, Valve, and Solenoid Valve. (Different Gauge Pictured Than One Designed for Up to 100 psi Used in Experimentation.)

The prototype shock tube was created to test the effectiveness of the piezoelectric sensors. These sensors had been tested first due to their responsiveness of 450 kHz and inexpensive cost of ~$40 USD/pack of ten sensors, including shipping and handling. They can be easily be placed on a surface by an adhesive material.

After promising results using one sensor, two sensors were installed to measure the time-of-flight shock speed in the tube. One sensor was at the end of the tube opening from the original setup while the other was placed one meter from the end of the tube for ease of calculating shock wave velocities. The sensor one meter before the end of the tube was set to the trigger of the oscilloscope. So, the starting time "zero" is when the sensor experiences a deflection, giving a signal over the set threshold of triggering the

oscilloscope. This way, when the oscilloscope records the shock wave data, the difference in position of the sensors can be divided by the time of the two peaks to find the velocity of the shock wave. The trigger threshold was set to where miniscule oscillations or small external forces, such as accidental movements, would not give enough energy to interrupt the data acquisition, setting off the trigger while tests were being performed. The trigger sensor was glued to a 3D printed housing clamp that let the sensor lay flat on the surface to keep itself from deflecting while in the tube. The shape of the clamp was designed in the shape of a rectangular prism having chamfered edges with six ¼-20 tapped holes for evenly distributed clamping pressure, as seen in Figure 6.

Figure 6

CAD Part Designs for Prototype Shock Tube Piezoelectric Sensor Clamp Halves: (a) Top, (b) Bottom

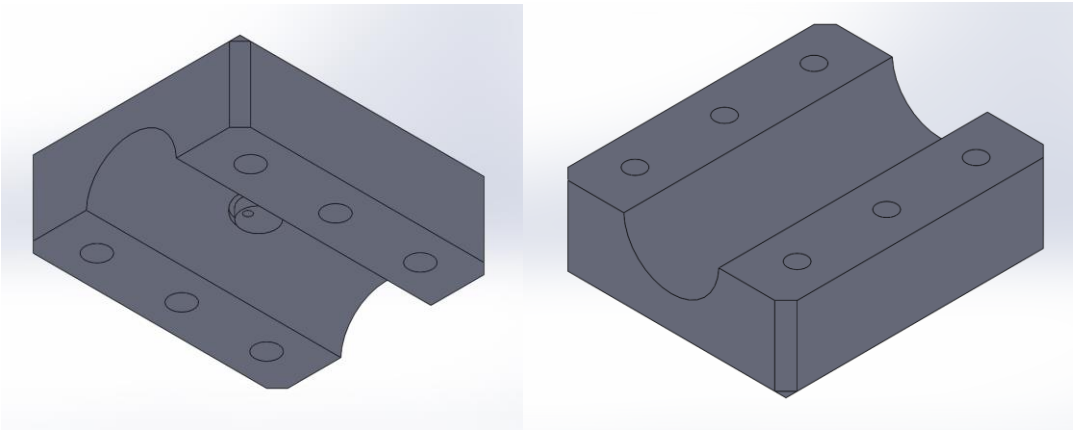

(a) (b)

The inside radius to fit over the pipe for the top and bottom clamp pieces were not exactly measured to fit the half circumference so that there would be a small gap, creating

more clamping force when tightening the screws. The clamp was designed so that the sensor would be flush to the wall of the pipe. The second trigger at the end of the open tube was glued to a small piece of printed material that caused it to lay flat instead of gluing the sensor straight to the curved surface of the tube. The finished product assembled can be seen in Figure 7.

Figure 7

Sensor Clamp Assembly with Parts (a) Assembled and (b) Disassembled

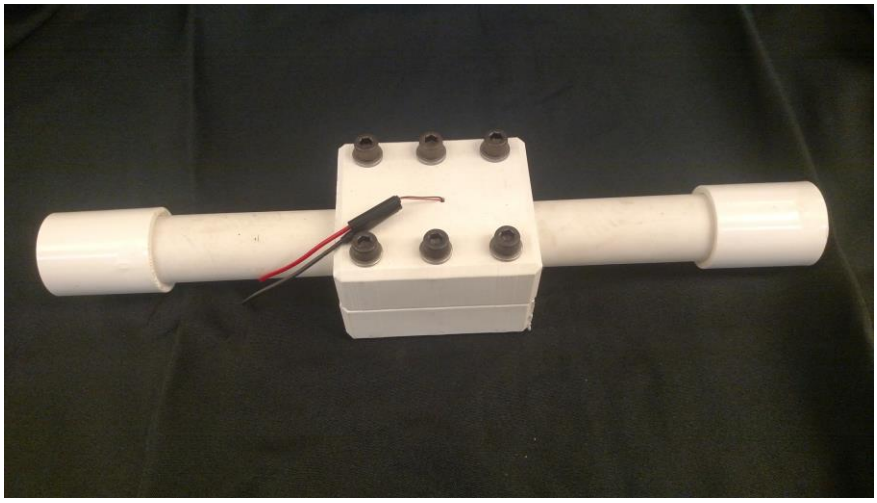

(a)

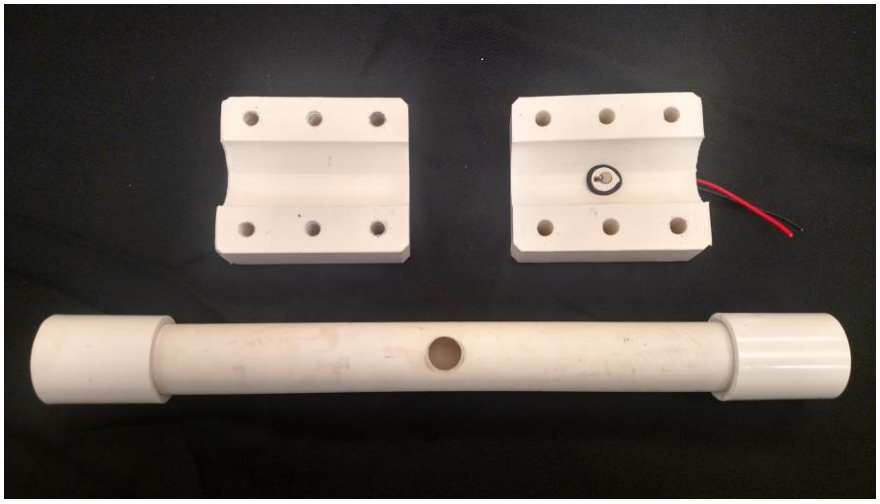

(b)

There are two considerations present when analyzing the results in determining if the sensors are adequate for use in the full-scale model. The first is to see if the sensors are precise in their measurements for a given initial driver pressure. The second is to see if the results follow the curve of the theoretical velocities beyond just obtaining a response. For the first consideration, the desired response is to see a sharp incline on the scale of tens of microseconds or less to know almost exactly when a shock wave passes. This is how we will know the sensors are suitable for lower supersonic Mach numbers anticipated in this shock tube design.

Initial experiments to test the sensors, need only show capability for time-of-flight measurements, so results (as will be shown) need not perfectly track the shock wave theory discussed above. In particular, the solenoid valve is a major consideration as compared to a diaphragm since it does not have a straight path for the driver gas to flow into the driven section. The different corners the gas travels through can cause energy to transfer into the walls and cause turbulent flow in its travel. This can cause the flow to become slower than

expected. The other reason the valve may not be suitable enough is the opening time. Though operated by a switch, the time the valve opens from the induced magnetic field may be slower than a diaphragm bursting. As shown in Figure 8, the desired result of seeing an increase of shock speed with increasing "burst" pressure was not achieved. Instead, the wave initiated by the solenoid opening propagated at essentially sonic velocity (~340 m/s) regardless of burst pressure, and with only slight dependence on driven section length.

Figure 8

Prototype Shock Tube Data with (a) Short (11 ft) and (b) Long (15 ft 4 in) Driven Sections

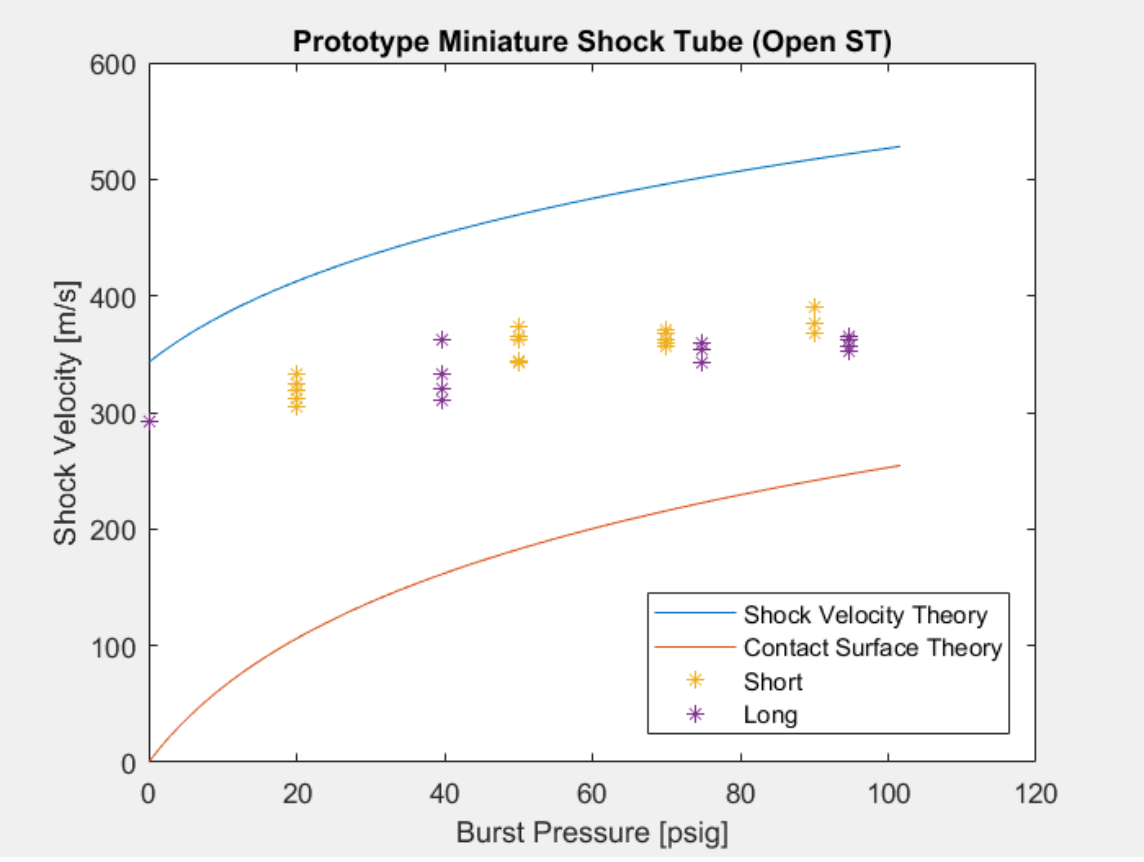

The data from figure 8 was collected by assuming the maximum crests of the peaks was a shock wave passage. Another oscilloscope, HP 54645D, was used which had software from the same era as the other but had more functions as far as capturing data with a more user-friendly start/stop recording device. The data appears to have a small progression in speed with increasing pressure, but it is not as easy to tell. Looking at the short and long tubes separately, an increase of speed can be seen but not to what is desired. Knowing the possible flaws in the design of the prototype shock tube, the setup may be causing a limit to the flow out of the valve, thus causing a low incline in the slope on the graph. Any pressures lower than 20 psig would not give a reading, making it harder to tell what the slope would look like when reaching the vertical axis intercept. Something noticeable on the graph is a distinction between the slopes of the short and long tubes. The short tube has given a steeper slope, as the longer tube doesn't seem to increase in velocity as much with higher pressures. This can be a result of the shock front losing energy quickly along the tube. If the data for the longer tube was shifted negatively about 20 - 30 psig on the x-axis the data would match up with the shorter tube. The data in Figure 8 shows a relatively tight grouping for the sensor response times. We can conclude the sensors are sufficiently precise for data acquisition, at least, for velocities near ~340 m/s.

Diaphragmless Shock Tube Study

Before moving on to the initial build of the full-scale shock tube, the design of the prototype shock tube stirred an idea to reduce cost, at least in long-term usage. This would be instituting a "diaphragmless" shock tube. Using a fast-acting valve would keep the cost down from negating diaphragm material. A few articles were researched on this design, and they were reported to have great success. [35] [36] [37] [38] The unknowing downside was not

knowing how a “diaphragmless” shock tube would act with the low pressures our experiment is using, as the sources researched used much of their research above 7 bar. This project will use pressures as low as between one and two bar, which can cause uneasiness in shock wave formation as we have already seen that a valve, though not developed for pulses, did not give the best results.

There was one valve, called the “Supah-Valve,” made from the Spudgun Technology Center that can be bought and is made from PVC.[39] The device works by opening a valve, causing the piston inside to push the air through the outlet. The total price of the most basic valve setup starts at $134.99 with only a ball valve and is mentioned to be as fast acting as a diaphragm. The downside to this is the complexity of design. It would be easier to purchase the valve than make it without the possibility of making an error in build, especially with high pressures. The manufacturer warns the consumer on the “Build Your Own” page and at the head of the website that PVC is not approved by the manufacturer to construct spudguns.[40] With all of this in mind it will be easier to construct what has already worked, especially knowing a plastic shock tube has already been developed and tested.

Full-Scale Shock Tube: Initial Building

Gathering Materials

The next steps finalize what will be used to build the full-scale shock tube. Most of our products came from McMaster-Carr website as their products are diverse and easy to obtain with quick delivery. Note that this project was not at any time sponsored by McMaster-Carr. Flanges would be used to connect the five-foot sections together. Creating flanges by hand was considered, but the best idea for this project is to find premade flanges

as they are easy to obtain and keep simplicity in shock tube development. Prices pertaining to each product can be found in *Appendix B*. The flanges chosen are reasonable in price considering they are schedule 80 PVC. The only downside is that the CAD drawings or description from McMaster-Carr did not indicate that the flanges are hollowed out from possible molds or manufacturing. Luckily the flange can seal at the inside diameter when assembled with a gasket. Our gaskets were also ordered from McMaster-Carr which were only a few USD each. ⅝-11 bolts and nuts with ⅝ inch washers were purchased for connecting the sections together. The bolts were chosen to be 3 inches long with a 1½ inch thread length to be long enough to pass through two flanges, two gaskets, and diaphragm material. The driver section has the same design as the prototype as it consists of a reducing bushing with the ball valve assembly attached to it.

Initial Design and Build

Another critical design decision was the shock tube support. Shock tubes will usually have more stabilized supports due to their mass, but we did not follow those considering the ease of operation, cost from the amount of material used, and storage space. The accepted design consisted of a US football goal post style support, as seen in Figure 9, which was made from a flowerpot filled with concrete and ¾ inch schedule 40 PVC tees, elbows, and piping.

Figure 9

Image of a Single Support Fork Made from ¾ Inch PVC

The tees and elbows had to be cut back a bit for the 3-inch PVC to fit snugly in the post. This design is simpler than a whole support assembly as supports can be added and subtracted depending on the length of the shock tube. A future consideration for the support design should be to drill a hole through the sidewall of the fork in a location that will reside within the concrete. That way, when the concrete sets, the post cannot slide out due to the concrete filling and grabbing the hole. to drill a hole in the post where it would fit in the concrete so in case the mix does not cure well, it would still be unable to be removed from the flowerpot. For information on building the different sections of the shock tube assembly, all manufacturing instructions are listed in *Appendix A.*

Partial Full-Scale Open Shock Tube

The next steps were building part of the tube itself for initial diaphragm studies. The sections were already determined by the piping and flanges, but the details of the tube were yet to be. In creating the tube for the diaphragm studies, the driver section had to be constructed. A 10 ft section of 3-inch schedule 40 PVC purchased was cut in half on a bandsaw, leaving the two halves for the driver section and extension section, as seen in Figure 10. The valve assembly attached to the driver section of the prototype shock tube was recycled for the full-scale assembly.

Figure 10

Driver Section of Full-Scale Shock Tube

A reducing bushing was found on McMaster-Carr and was glued to the pipe with the help of a coupling. The flange was glued onto the other side of the pipe. While

constructing the tube it was a good idea to first make the five-foot driver section with one extension section having an open end to test different diaphragm ideas. The extension section was needed to insert diaphragms between the flanges of the driver and extension sections. This was the simplest section to create as it requires a five-foot length of PVC and two flanges glued to the ends, as seen in Figure 11.

Figure 11

Extension Section of Full-Scale Shock Tube

With these two sections, the diaphragms can begin to be tested.

Chapter 5

Diaphragm Study

Transparency Films

In searching for a diaphragm material, we stumbled upon a pack of transparency films used for overhead projectors. These films are 8.5 by 11 inches and are 0.0035 inches thick. Our discovery was a good find to test as transparency films can be bought as low as roughly ten USD for a pack of 100. This can provide ~10 cents per shot, assuming one diaphragm per sheet.

Diaphragm Geometry

The first idea is to determine what shape would give proper sealing and stay in place while sandwiched between the flanges of the shock tube. The first idea was to replicate the silhouette of the cross-sectional area of the flanges. This consists of a circle with a 7.5-inch radius with four smaller circular cut outs for the bolt holes as seen in Figure 12.

Figure 12

CAD Rendering of First Diaphragm Design

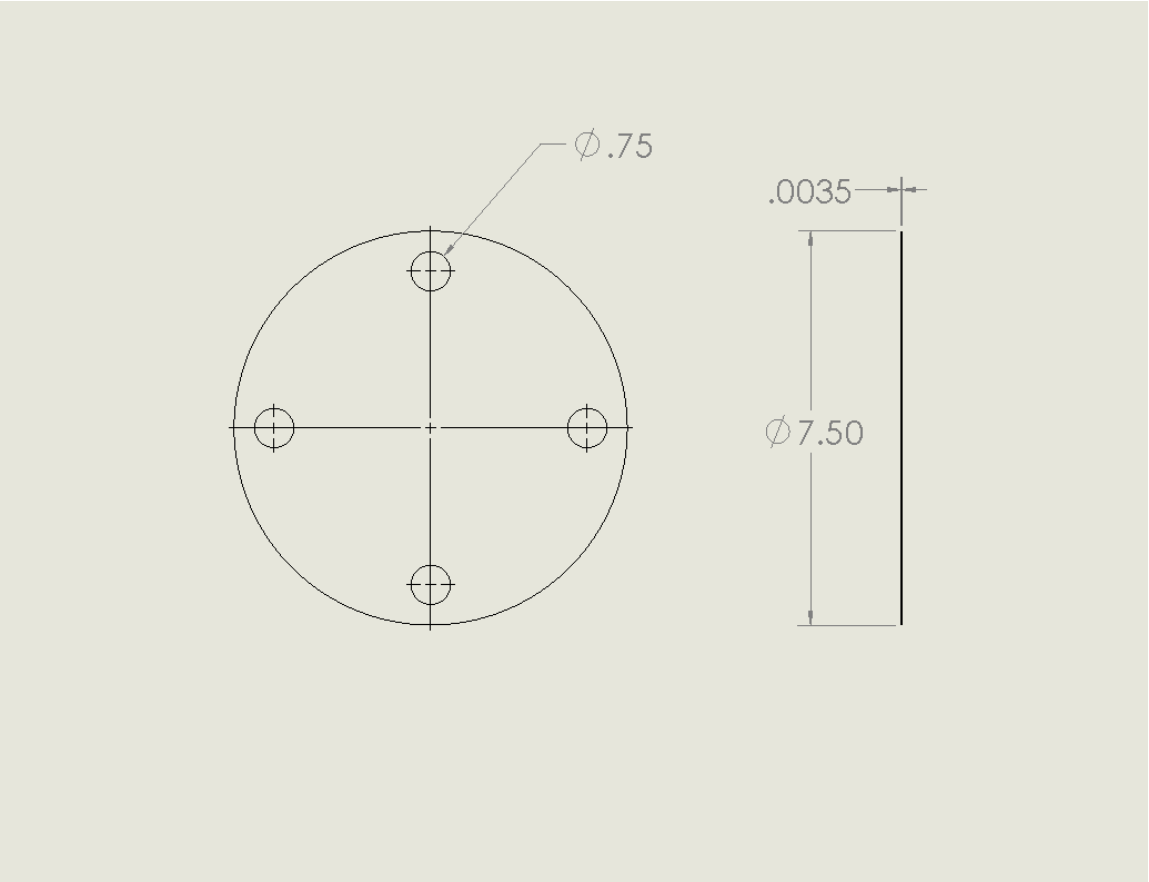

The first few diaphragms were traced by hand using one of the gaskets and cut out with a razor blade and scissors for the bolt holes and circumference. These diaphragms did seal properly, but the edges cut out were jagged and could easily cause the diaphragm to rip and void it for use.

The next idea was to determine if the films were capable of being cut by a CO_2 laser cutter since our institution has one. After acquiring information on the material of the film and determining it was safe for laser cutting, it was determined that its composition, polyethylene terephthalate, was safe.[41] Since the films are thin, they can be cut at a low

power setting. There seems to be a point at each power where the film cannot be cut, or even etched with the cutting mode selected. All the diaphragms cut were cut at the same setting and power from this design to the final design. Besides this point, the diaphragms were able to be cut with smooth edges without releasing poisonous gases or combusting. After making a few of these diaphragms, it became apparent that these diaphragms can be cut slim enough to cover the needed sealing area and save enough room for another diaphragm to be cut on the same sheet. As compared to 7.5 inches, the width can be cut down to 4.36 inches, as seen in Figure 13.

Figure 13

CAD Rendering of Second Diaphragm Design

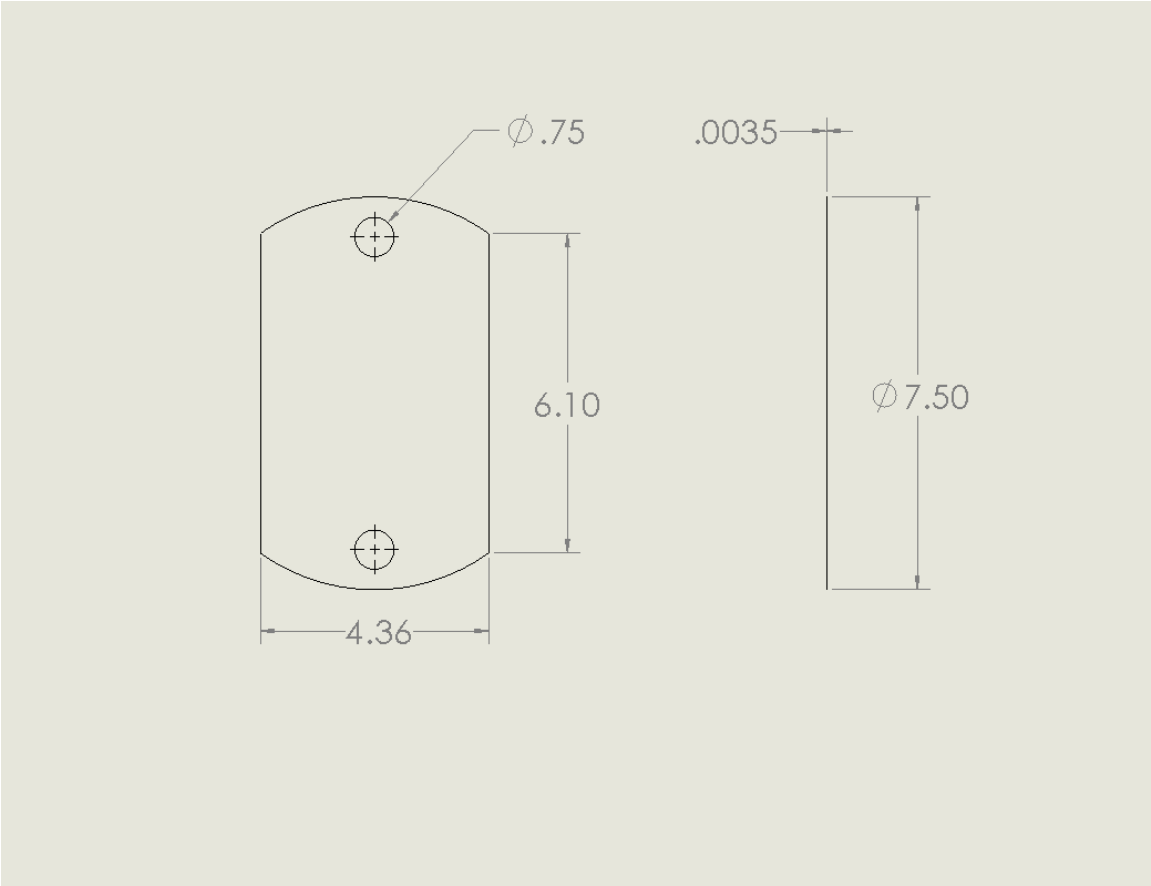

This will cut the cost of diaphragm making to half the cost as it was before from ten to five cents each. A critical purpose of this project is to make this shock tube inexpensive to build and operate so any institution can have one of their own. The final adjustment to this diaphragm was making the edges of the diaphragm square to show that they can be made by hand and still work, as seen in Figure 14.

Figure 14

CAD Rendering of Third and Final Diaphragm Design

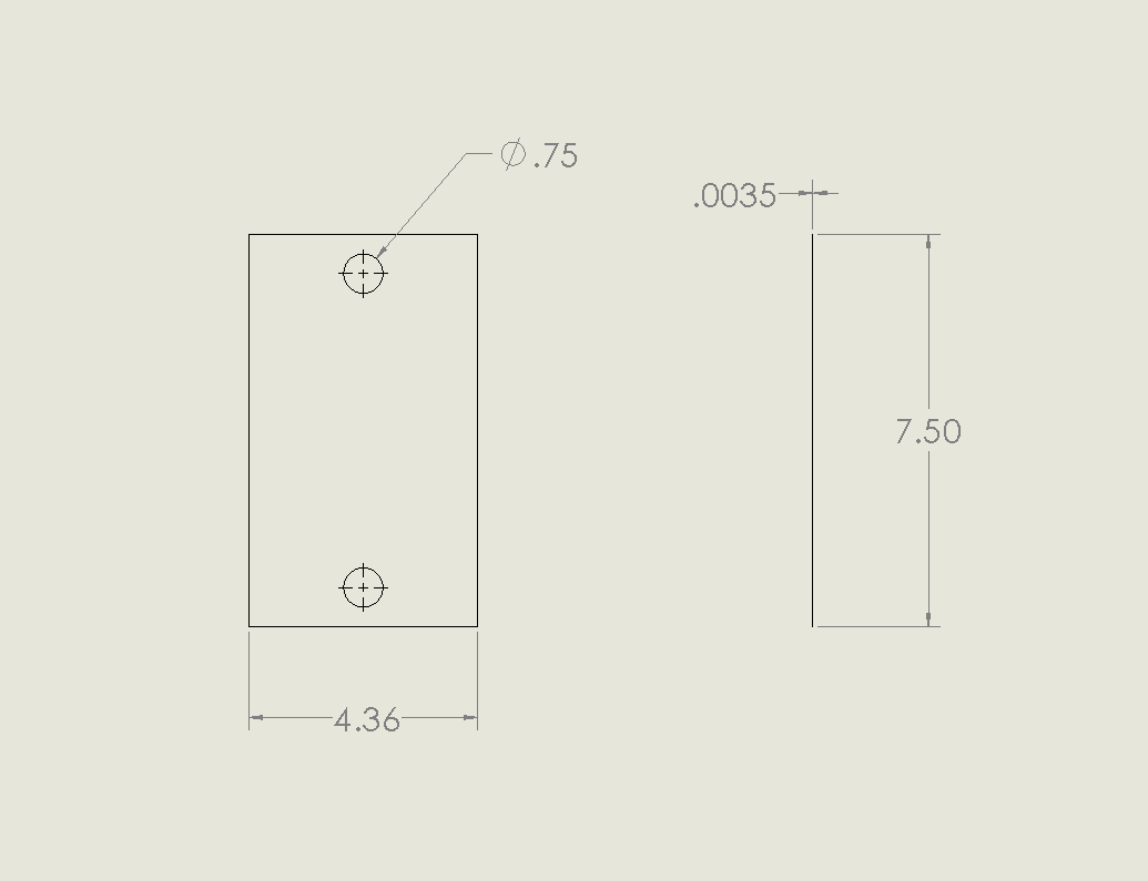

Another critical purpose of this project is to prove a shock tube can be built inexpensively with minimal tools to the point where one can even be made in a home-owner's garage or shed. This simple creation of a diaphragm, though done with expensive technology can also be conducted by hand with a hole punch, such as a cork punch, ruler, and a pair of scissors after tracing the shape of the gasket bolt holes.

Burst Statistics

The bursting pressure was tested for the transparency film diaphragms, and each test resulted in about 60 psig (~75 psia). Four tests were recorded for the diaphragm with

four and two bolt holes each. These are the initial tests done, but as the process of installing diaphragms for testing became swift, the bursting pressure for the diaphragms stayed in a range of 60 to 70 psig for each run, as represented in Table 1. For the rest of the project, most shots were fired at ~60 psig These are quality results as the average and accuracy of the diaphragm bursting pressures are acceptable for further testing and manipulation to the diaphragm geometry. To understand the stress and strain experienced by these diaphragms, the first two-bolt diaphragm seen in figure 15, noted as N/A in Table 1, was preserved since it did not burst. It was taken out due to leakage as it was the first attempt to burst this material. Luckily, the leakage did not continue and was an operational fault. As seen in Figure 15, the diaphragm bulges with the amount of pressure it experiences. With this diaphragm, the bulge protruded about an inch at around 40-50 psi.

Table 1

Initial Tests of Transparency Film Diaphragms with the Open Shock Tube

	Two-Bolt Diaphragm		Four-Bolt Diaphragm	
Diaphragm	Burst Pressure [psig]	Burst Pressure [psia]	Burst Pressure [psig]	Burst Pressure [psia]
1	N/A	N/A	60	74.7
2	70	84.7	64	78.7
3	64	78.7	62	76.7
4	65	79.7	62	76.7

Figure 15

Transparency Film Diaphragm Bulged Before Bursting

When the diaphragms burst, they all gave repeatable bursting patterns, as seen in Figure 16. There were no diaphragms that lost material. Each diaphragm burst at ~60 psi and created two to four petals, with the rip beginning at the center of the diaphragm.

Figure 16

Transparency Film Diaphragm After Bursting

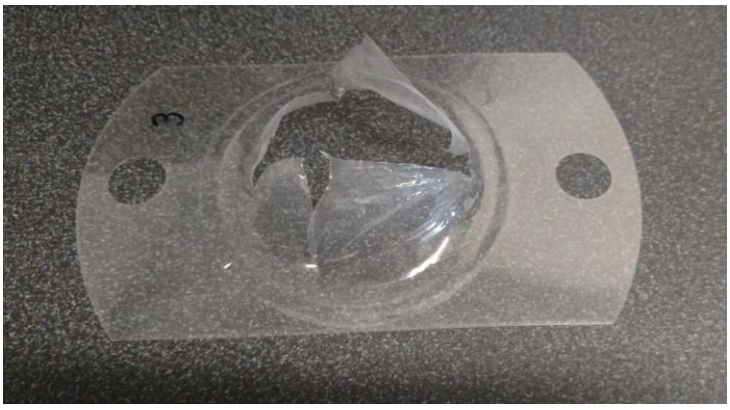

Scoring Attempt

The next step was to score the diaphragms, so the bursting pressure could be varied and controlled due to the deepness of the cuts. The first attempt here was to replicate what other sources have done in making an “X” score across the diameter of the diaphragm as seen in Figure 17. This was done by making the score on Solidworks with a very small thickness since the laser cutter would not register lines when cutting.

Figure 17

CAD Rendering of Third Diaphragm Design with a Laser Scoring in the Center

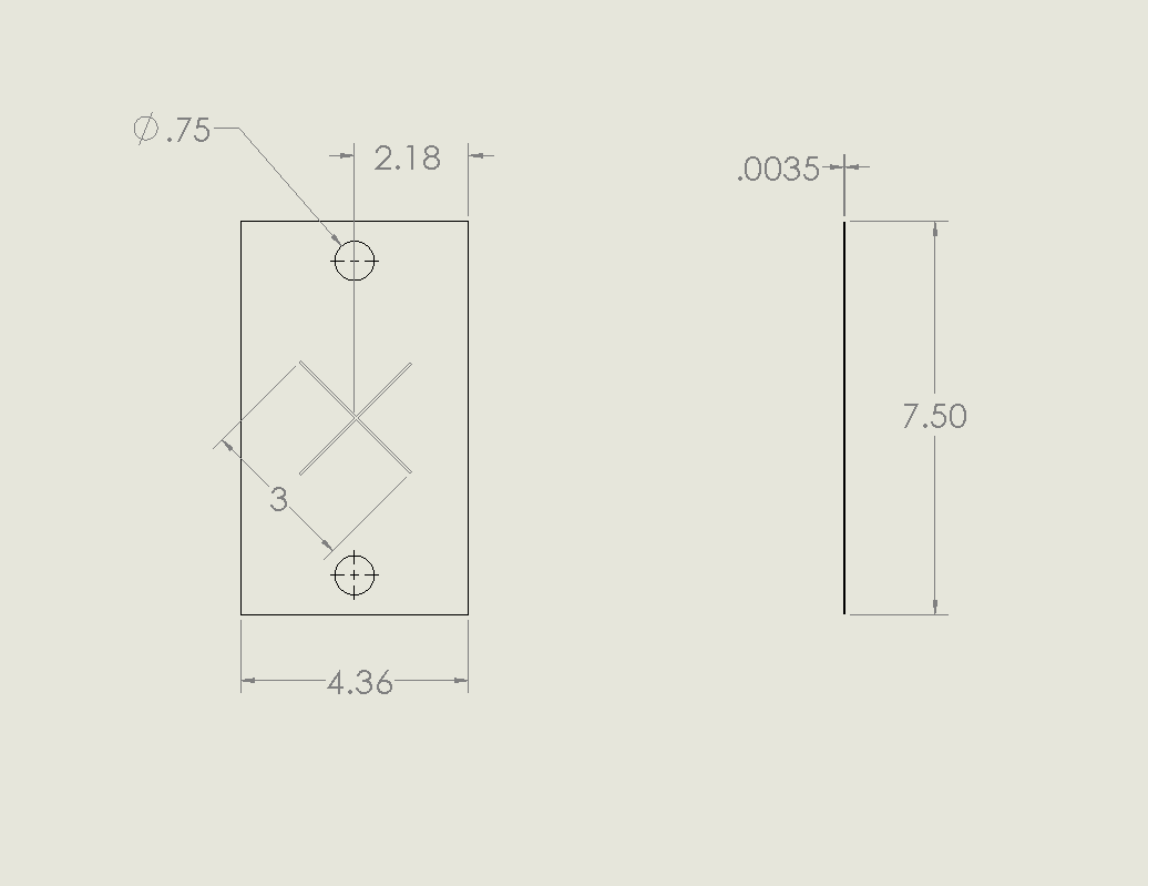

The first attempt was done by scanning (etching) at the highest rate with a 15% power setting. At the end of the cut, the laser melted through the material, as seen in Figure 18. The next attempt was to cut the perimeter of the score at 15% power and the fastest speed laser cutting speed possible (350 mm/s). These diaphragms gave a better result than the ones that were etched, but they were still inadequate. The edges where the laser stopped for a fraction of a second to switch directions gave an exposure long enough to melt through the material as seen in Figure 19.

Figure 18

Laser Etched Attempt of Scoring Transparency Film Diaphragm

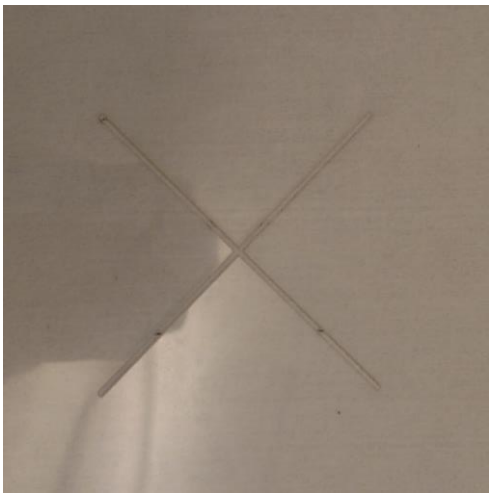

Figure 19

Laser Cut Attempt of Scoring Transparency Film Diaphragm

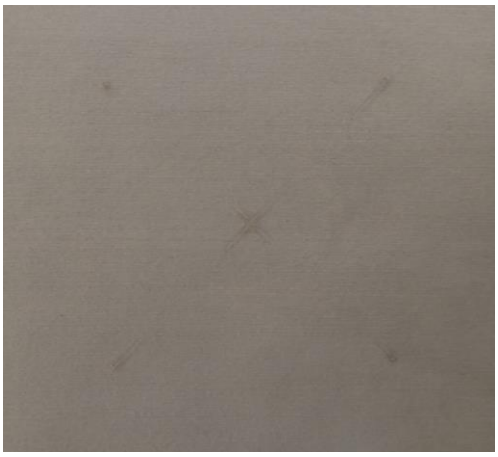

Attempting to ease the problem of too much exposure, the “X” score geometry was replaced by a three-quarter inch diameter circle score placed at the center of the diaphragms. The difference of these tests was that each score was created by varying the power while keeping the same height difference and speed. This seemed to have the same effect that the variation of height with constant power did. There is a very small range of power variation where the diaphragm can be scored without cutting through or only warping the sheet slightly due to slight melting. The sheets need to be laid flat with no wrinkles, dimples, or folds. Unfortunately, the cutting process of the circle scores did not prove to yield favorable results.

The cutoff of power at this height turned out to be just over 10%. Table 2 gives an almost linear burst pressure to power slope, but the sensitivity of the material to laser cutting and short range showed this was not a reputable method. The starting and stopping

points of the laser cuts were given more exposure, leading to more melting and potential holes.

Table 2

Scoring Transparency Films with Power Variations on the Laser Cutter

Power [%]	Burst Pressure [psig]
8.5	30
9	8
9.5	6
10	4

Note. Laser cutter is at a set height. This is meant to understand scoring ability and power to burst pressure relations on circular scores that are three quarter inches in diameter.

The last attempt was to laser etch a score consisting of a very thin line 1.5 inches long. Laser tests were done to find the range of heights at 20% power. As the others, this did not do well, so further attempts to make the scored transparency films by laser cutter were abandoned. For varying bursting pressures in a single diaphragm shock tube, transparency films are not a good way to go unless the scoring can be achieved mechanically.

After deciding scoring on a laser cutter was not adequate for transparency films, another method for varying bursting pressures was decided. Instead of scoring, diaphragms that have low bursting pressures can be layered to vary bursting pressures linearly. Paper is very thin and not as strong as the transparency films are. Paper is also laser cuttable, making itself a good candidate for this technique. Different inexpensive, easily accessible

types paper were researched to determine if their compositions would be suited for laser cutting and not release toxic fumes when burned. The different papers chosen were parchment, freezer, wax, and construction paper.

Paper Diaphragm Study

Parchment paper is a non-coated, non-sticking paper used for cooking and baking. Freezer paper is like parchment paper but is coated with wax on one side in preserving meats and is a bit thicker than parchment paper. Wax paper is just like parchment paper but is coated with wax on both sides, making it a waterproof material. Construction paper is a tough paper that is usually used in arts and crafts for its color and texture. The prices are $5.49, $3.29, $1.59, and $2.99 for consumer units of the parchment, freezer, wax, and construction paper. The parchment paper is 65 ft x 13 in to make roughly 224 diaphragm sheets. The freezer paper is 50 ft x 15 in to make roughly 240 diaphragm sheets. The wax paper is 75.6 ft x 11.9 in to make roughly 240 diaphragm sheets. The construction paper is 96 sheets of 9 x 12 in to make 192 sheets. The cost for each diaphragm will be $0.025, $0.014, $0.007, and $0.016 for the parchment, freezer, wax, and construction paper.

Each paper was tested in the laser cutter at 15% power and with a laser cutting speed of 30 mm/s. This was done at a laser height difference of 10 mm from the paper. Each type of paper proved to not start a fire or emit any toxic gases. The parchment paper was easy to roll out on the laser cutting bed and lay flat without any paper moving as the laser cutting head is equipped with a nozzle for spraying cold air. Cutting the freezer paper was different as it attempted to keep its curled shape as it was rolled in its packaging, especially when rolling the paper closer to the middle of the roll. Placing it in the laser cutting bed was simple, but it was supported down by acrylic pieces in opposite corners to

keep it as flat as possible. Acrylic was used since it is laser cuttable in case hit by the laser beam. The wax paper was easy to cut as well as it laid flat on the cutting bed, as was the construction paper since it is already flat in its packaging.

Parchment Paper

Burst pressures of were tested to determine if the different types of paper, if any, were suitable for being reliable and inexpensively used. Each type of paper was burst in groups of one to five in a stack for discovering durability, tear characteristics, fatigue characteristics, and burst pressures. The first type of paper tested was the parchment paper. This paper fit snug between the clamped gaskets without tearing the material around the inner diameter, where most of the clamping force is transmitted due to the shape of the flanges. The burst pressures were not in the ranges desired as they have low bursting pressures, as seen in Table 3. The pressures weren't too low as to use so much material on higher pressures, but the desired change in pressure should use less material for shots for cost, manufacturing, and cleaning.

Table 3

Parchment Paper Bursting Pressures from One to Five Layers of Sheets

Sheets in Row [#]	Burst Pressure [psig]	Burst Pressure [psia]
1	2	16.7
2	16	30.7
3	18	32.7
4	26	40.7
5	28	42.7

The tear characteristics of the paper had tearing around the edges from the shock tube inner diameter since paper isn't stretchable, unlike the overhead sheets. Using one sheet only caused the material to fold over as the gas passed by, showing it wasn't strong enough to rip entirely. The diaphragm did not lose any material from the tearing. As more sheets were added, the diaphragms started to lose material as the shock wave had to push its way through the material as seen in Figure 20.

Figure 20

Burst Parchment Paper Diaphragms

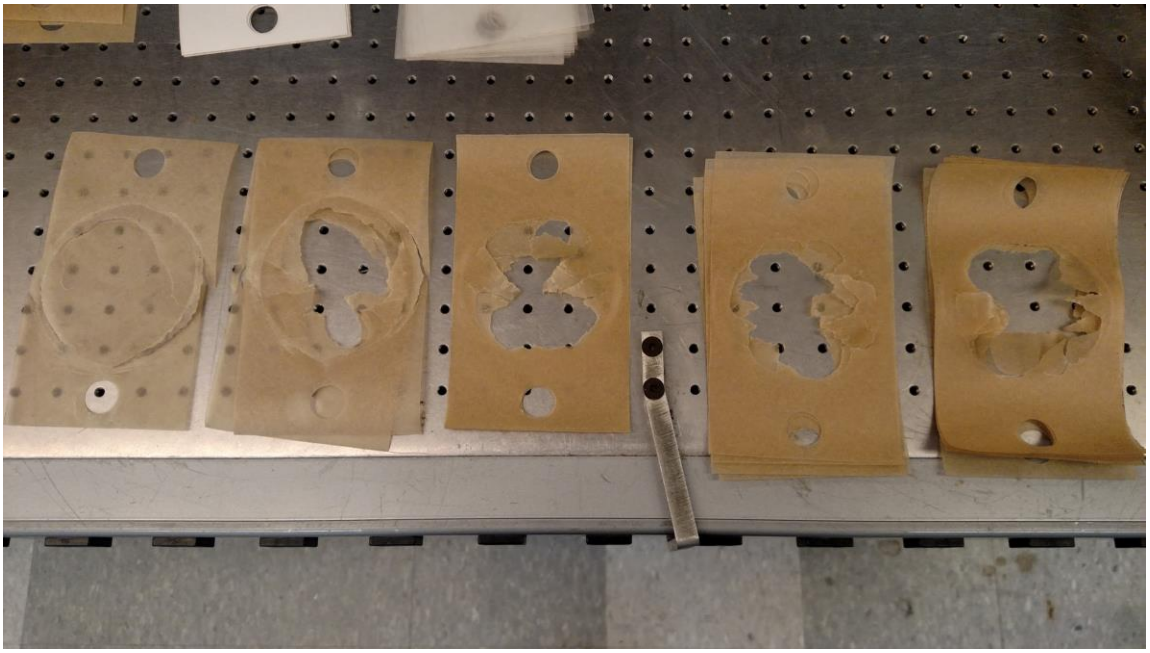

Note. Ordered from left to right: one to five layers.

The more layers in a stack, the more the gas pressure took out a cross section piece and pushed it through the tube. As far as housekeeping, the paper has a static attraction with the plastic surfaces of the tube, making it a bit more tedious to prep the tube for the next shot.

Freezer Paper

The next paper tested was the freezer paper, which had a noticeable difference in structure and durability compared to the parchment paper. This freezer paper coating was plastic instead of wax, which has the possibility of making it stronger, comparing it to the plastic overhead sheets. This paper proved to be better than the parchment paper as its bursting pressures were higher, as seen in Table 4.

Table 4

Freezer Paper Bursting Pressures from One to Five Layers of Sheets

Sheets in Row [#]	Burst Pressure [psig]	Burst Pressure [psia]
1	10	24.7
2	16	30.7
3	32	46.7
4	48	62.7
5	50	64.7

The freezer paper was able to reach 50 psig for the trial with a five-sheet layer. The bursting characteristics were very similar to the parchment paper. The single sheet did not lose any material but was folded after bursting, as did the two-layer diaphragm. The two-layer diaphragm can lose material as noticed in experimentation. Once there were three sheets, material was lost and shot through the tube. In Figure 21 the diaphragms start to

burst in pedal shapes with the pedals mostly being torn off and sent down the tube. The cleaning was easier as the paper was more robust and did not stick to the walls of the tube. Most, or all, of the pieces could be blown out with one breath.

Figure 21

Burst Freezer Paper Diaphragms

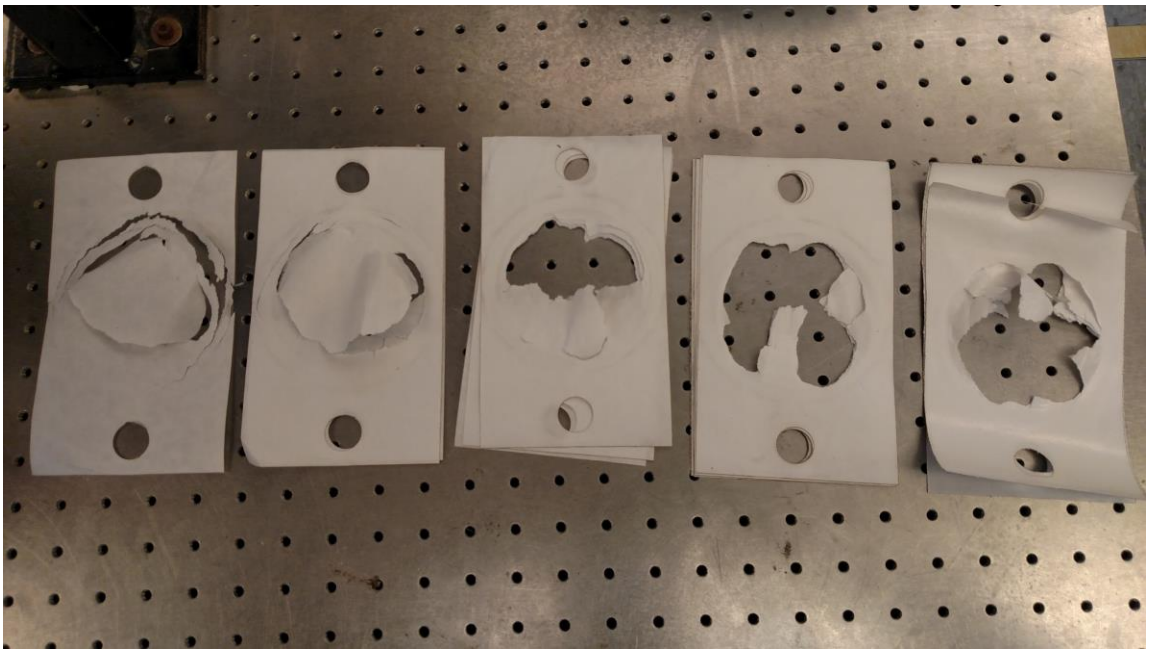

Note. Ordered from left to right: one to five layers.

Wax Paper

Testing the wax paper was next. Since the paper was brittle when folded, it did not initially seem to be a good candidate but was tested for its bursting pressure and characteristics. It did have enough strength to be pulled from side to side, compared to the other papers. Since both sides were coated in wax, the paper has a great chance of sealing air from going through the material. Unfortunately, this paper yielded unsatisfactory bursting pressures.

As seen in Table 5, the bursting pressure of a 5 layered diaphragm is only 13 psig. This would exaggerate the amount of production and cleaning if used, which makes it an unfit candidate for a diaphragm. The bursting characteristics tend to be like the others. One sheet kept all its material and folded as the air passed by, while the other shots took pieces off and eventually started creating pedals.

Table 5

Wax Paper Bursting Pressures from One to Five Layers of Sheets

Sheets in Row [#]	Burst Pressure [psig]	Burst Pressure [psia]
1	2	16.7
2	5	19.7
3	6	20.7
4	12	26.7
5	13	27.7

The single sheet in Figure 22 does have tears on the side, but it did not seem to leak gas from the flange setup. What is very interesting is that the bursting characteristics tend to be dependent on the number of sheets rather than the bursting pressure. The freezer paper bursting pressure was much higher compared to the wax paper, but the way the diaphragm tore was the same for each.

Figure 22

Burst Wax Paper Diaphragms

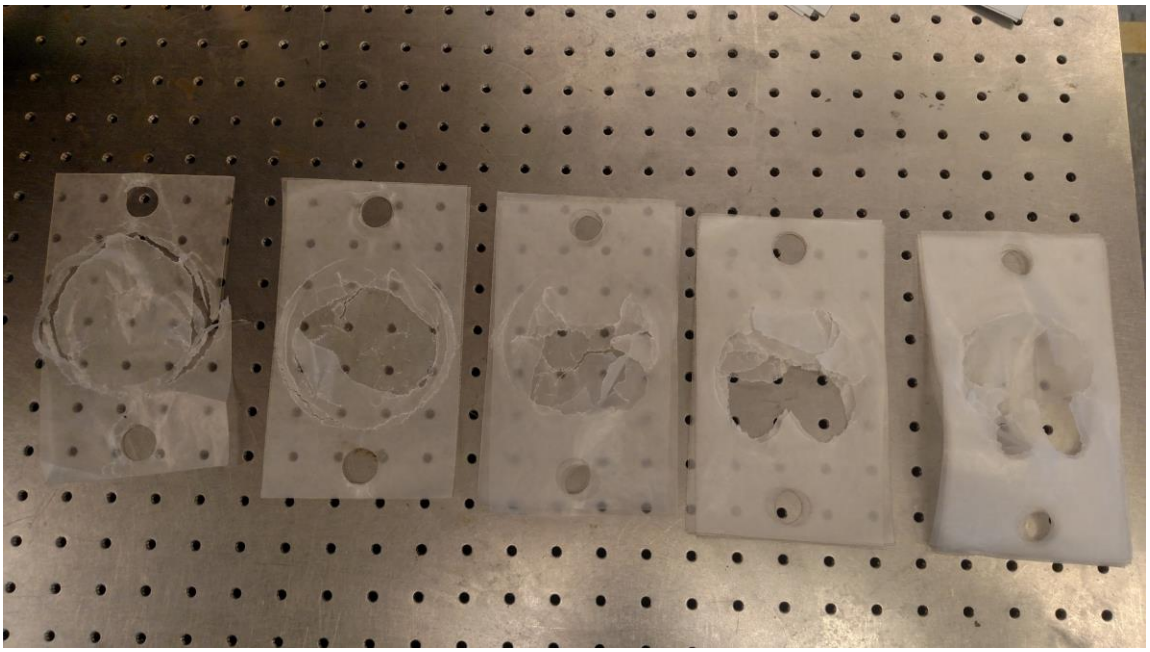

Note. Ordered from left to right: one to five layers.

Construction Paper

The construction paper was tested last. This paper was the thickest and had the coarsest texture out of all the others, which may be able to assume a higher bursting pressure. Since construction paper is made mostly from wood pulp, the material consists of fibers. This may cause the paper to not seal properly through its surface. This difference may result in lower bursting pressures.

The bursting pressures were like the parchment paper, as seen in Table 6. This paper has the most linearity in bursting pressures out of all the papers for a trial testing. Though it is optimistic it will be for other tests, the assumption should be tested further for any deviation as the other papers do not have a definite burst pressure besides one-layer sheet.

Table 6

Construction Paper Bursting Pressures from One to Five Layers of Sheets

Sheets in Row [#]	Burst Pressure [psig]	Burst Pressure [psia]
1	3	17.7
2	9	23.7
3	14	28.7
4	19	33.7
5	25	39.7

Again, the bursting characteristics are the same as the others. It has the same exact rip effect as the other papers, but there was more material still secured to the diaphragms after bursting compared to the others, as seen in Figure 23.

Figure 23

Burst Construction Paper Diaphragms

Note. Ordered from left to right: one to five layers.

From all the papers tested in the trial, freezer paper gave the best results for spanning a reasonable range of burst pressures. It gave the highest bursting pressures for the number of papers used, sealed correctly, did not rip under clamping force, can be easily cleaned, and ideally has the lowest cost per shot. The only difficulty with this paper was manufacturing as it tried to keep its rolled packaging shape. This paper was assessed further for better statistical information and testing the piezoelectric sensors for their accuracy and sensitivity in response time.

Freezer Paper Statistics

As seen in Table 7, the freezer paper was to be burst roughly five times for each different number of layered sheets with the open shock tube. Shooting 1 and 2 layers did not create sufficient response to trigger a time-of-flight measurement. With the two-layer

paper stack, the oscilloscope showed at most two miniscule bumps on the trigger sensor, with nothing on the others. The oscilloscope was only able to record data for at least three-layered shots with the open shock tube. The waveform of the shots of three to six layers were analyzed by the peaks made, which will be discussed later in the open and closed shock tube sections. The burst pressures were calculated with each waveform recorded to find the standard deviation of the layered shots.

Table 7

Quantitative Characteristics of Freezer Paper Diaphragms in Open Shock Tube

Sheets	Shots	Average Burst Pressures [psig]	Standard Deviation [psig]
3	5	36	4
4	6	48.83	2.34
5	5	60.4	7.5
6	5	79.8	5.71

The closed shock tube was able to capture shock speed with at least two layered shots with 23 psig as the lowest recorded bursting pressure. The waveforms of the shots were analyzed by the peaks made, which will be discussed in the open and closed shock tube sections.

Table 8

Quantitative Characteristics of Freezer Paper Diaphragms in Closed Shock Tube

Sheets	Shots	Average Burst Pressures [psig]	Standard Deviation [psig]
2	5	24.2	0.75
3	9	39.78	3.82
4	6	56.83	3.89
5	5	75.6	6.53
6	5	90	3.52

The freezer paper bursting statistics were nearly the same in the closed as in the open shock tube. There is some difference, but at the same time the bursting pressures will vary for each shot, giving the statistics a range as a better way to determine burst pressure than using consistency.

In the paper diaphragm testing out of what was used in this project, freezer paper is the way to go both in terms of cost and manufacturing. A laser cutter is a great way to manufacture diaphragms, but if an institution does not provide such a luxury, using scissors and a hole punch, which are listed in *Appendix B,* can provide a method of hand constructing them.

One more type of diaphragm was tested to understand its characteristics. Instead of layering only one type of diaphragm material, a sheet of aluminum foil was placed between two freezer paper sheets. The characteristics weren't different than expected from the previous diaphragms, as seen in Figure 24.

Figure 24

Burst Diaphragms of Freezer Paper, Aluminum Foil, Freezer Paper Layered Sheets

The noticeable characteristics are the burst pressures and their deviation. Its burst pressures were roughly 10 psi less than the three-layered sheets of only freezer paper, which tells us aluminum foil is very weak depending on the thickness of the foil. A thicker foil used for possible industrial application may suit better for bursting. The burst pressures were about two to five psi higher than the two layered freezer paper sheets, so the foil participated in strengthening the threshold of the diaphragm. The deviation was low compared to the other freezer paper layered diaphragms, which were closer to three or four. Considering that the two layered freezer paper sheets had a very low standard deviation of 0.75 psi burst pressure, the aluminum foil may have caused some variation in burst pressures.

Chapter 6

Full Scale Shock Tube: Final Build

Piezoelectric Sensor Assembly

Prior discussions inform construction of the full driven section. Earlier, when making the prototype shock tube, an idea of making a sensor assembly was to use a plastic screw that was 3D printed to place the sensor on and tap a hole for the screw to be placed in. Unfortunately, the ¾ inch PVC wall was not thick enough to place a screw in firmly. Since 3-inch PVC walls are thick enough for this, the idea can now be introduced into the project. A nylon screw on McMaster-Carr's website was able to be purchased for one dollar each. Now each sensor is made for six dollars. Three-foot-long BNC cables with BNC solder connectors attached were acquired from the Department of Electrical and Computer Engineering to connect the sensor screw assembly to the data acquisition. Thin wires, about 28 gauge, were used to complete this connection. The sensors were then able to be tested in the full-scale shock tube.

Along the end section there is a sensor placed at two feet from the side that connects from the end section due to the theoretical calculation of the shock wave development length at top velocity of 630 m/s. A half-meter on each side of this sensor are sensors used to calculate shock velocities throughout the end section as seen in Figure 25 (a). The extension sections are five feet in length with flanges on each side.

Figure 25

Piezoelectric Sensor Setup Shown with (a) the Leads and BNC Cable Shown, (b) a Closeup Look at the Sensor Screw Assembly

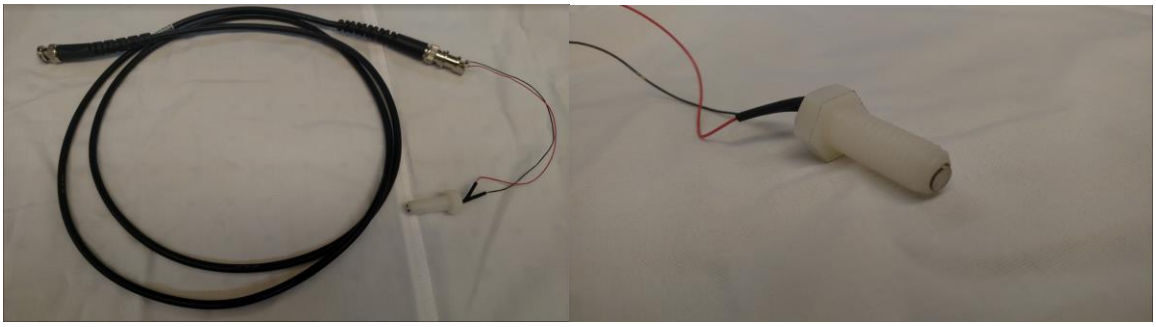

(a) (b)

Testing the Open Shock Tube

The first shock tube testing was with the end opened. As a precaution, ear protection is a necessity as the open-ended shock tube causes the propagating acoustic waves from inside the tube to transfer a large portion of its energy into the surrounding air. Also, the force of the air pushing itself out of the tube causes the shock tube to recoil. Having a vibration dampener on your pressure gauge would be beneficial for more accurate readings. It is also a good practice to have no participants or bystanders to be in front of the opening of the tube to prevent physical injury or hearing loss.

The first tests were done with the transparency films and some tests were done to capture the waveforms on a set time and voltage division. For these tests, only two sensors were installed on the shock tube, with one at 12 feet from the diaphragm and one 0.5 meters after the first sensor. It took some time to adjust the oscilloscope's parameters to find the shock waves, but it was eventually able to obtain disturbance readings. The results did not come out as well as they did from the prototype data collection. There were a couple

noticeable peaks, but after the peaks there was a wall of noise that was indistinguishable as seen in Figure 26.

Figure 26

HP 54645D Oscilloscope Data from Two Sensors 10.36 and 12 ft from the Diaphragm in Open 20 ft Shock Tube

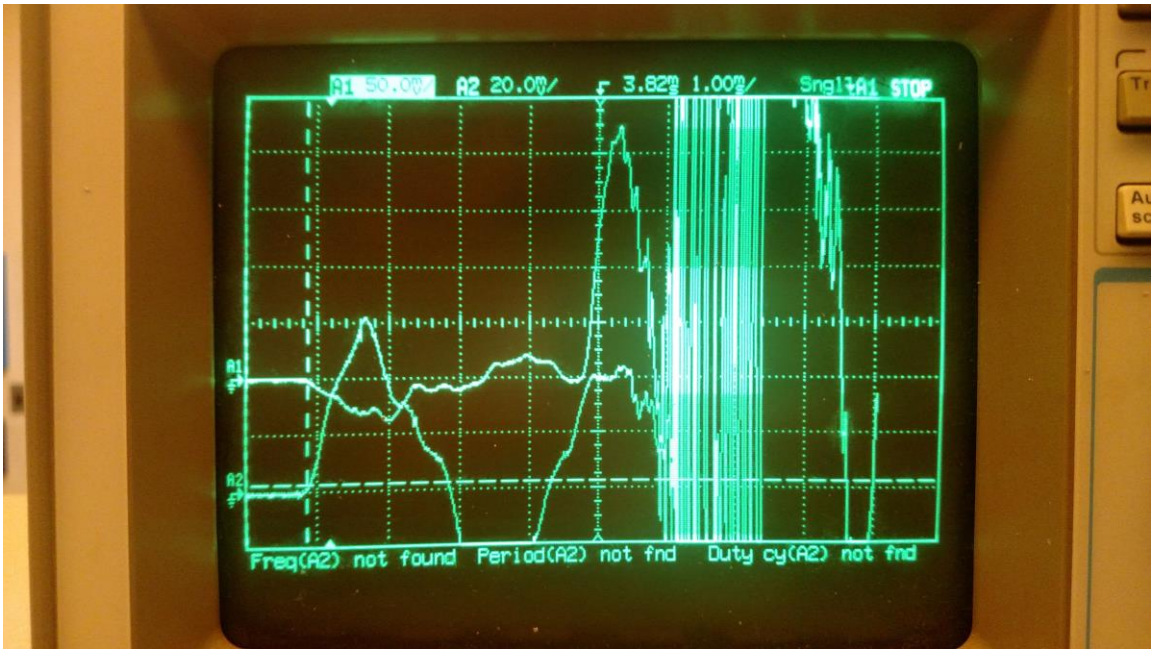

Our old oscilloscope was not able to give us what we needed since the waves needed to be distinguished from each other as the data was only shown in green. There was also difficulty in having an oscilloscope without today's creature comfort capabilities (such as having a USB port and difficulty figuring out screenshot capabilities), so it was easier to eventually switch to the 1 GHz, 4GSa/s Agilent Infiniium DSO8104A digital oscilloscope running Windows XP and the capability to easily distinguish waveforms by

color. After some testing and fine tuning, the oscilloscope was able to capture the waveforms.

To better compare the results with theory, another sensor was placed 0.5 meters ahead of the sensor at the 12-foot mark. With this, two different time intervals are recorded, which may give two different values if the shock wave is decelerating. Also, the first sensor is ahead of the theoretically calculated shock wave development length, so it will be interesting to see what values are obtained.

The open shock tube results were surprisingly close to the theoretical values. The shock wave passages were calculated by referencing the first noticeable spike in the data going towards a crest in the peaks. The first sensor (yellow) disturbances were easier to determine, but others, like the second (green) and third (purple) were not easy to gauge where the biggest spike would be located. This can be seen in Figure 27.

Figure 27

Open 20 ft Shock Tube Data of 4 Layered Sheet of Freezer Paper Diaphragm Burst at 51 psig

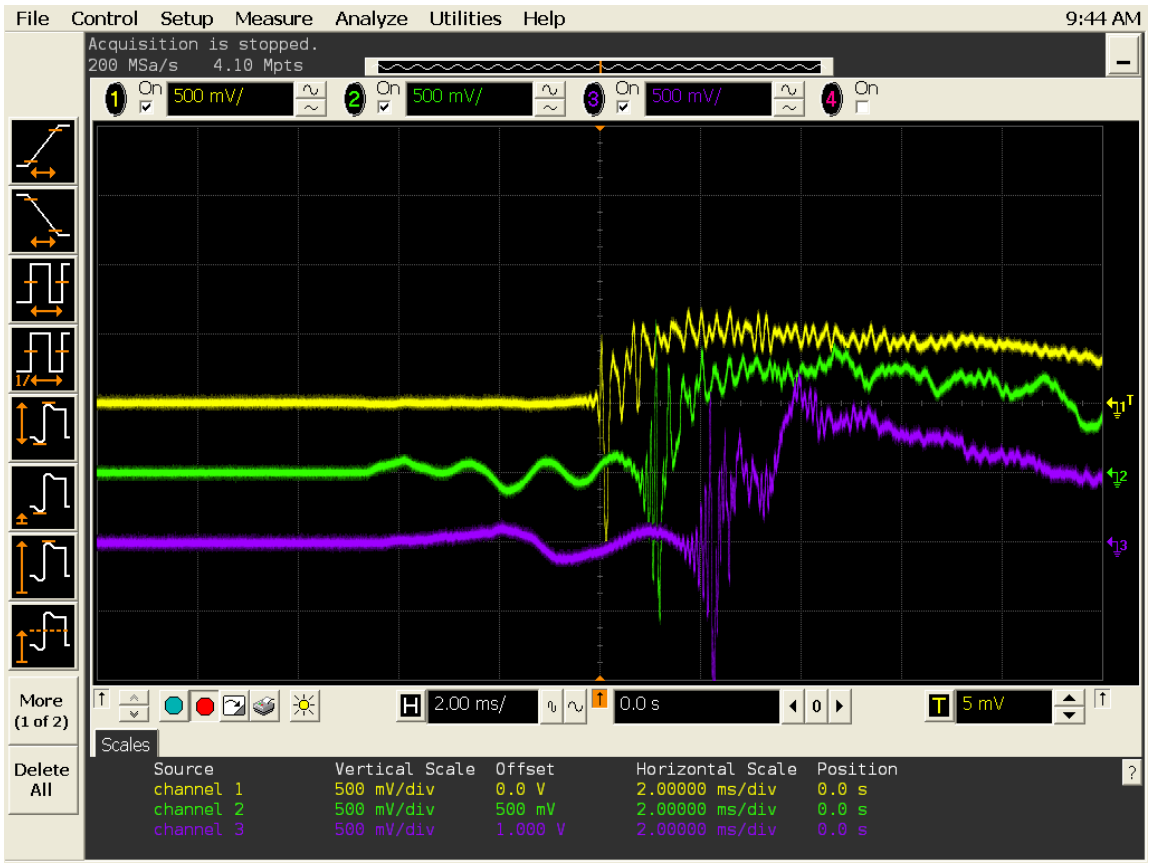

Note. Sensor colors by distance from diaphragm location are: Yellow (10.36 ft), Green (12 ft), Purple (13.64 ft).

The farther the sensors are from the diaphragm the harder it is to tell exactly when the shock wave passes by. We were unable to find the contact surface anywhere in all the data for each shot. Times of passage for the contact surface were calculated from theory to find out exactly where it would appear on the waveforms, but no peaks or added noise was seen.

In case shreds of paper were interfering, some overhead transparency sheets were shot, but still nothing was seen over the disturbance. Measured signal voltages grew swiftly

at the shock wave passages but steadily declined as time went on. When the paper diaphragms were shot much of the data experienced patterns without being related to the burst pressure or the number of sheets in a layer. Some experienced large spikes 10 to 20 milliseconds, as seen in Figure 28, after the shock wave passage, which could possibly be chunks of paper hitting the sensors.

Figure 28

Open 20 ft Shock Tube Data of 6 Layered Sheet of Freezer Paper Diaphragm Burst at 79 psig

Note. Sensor colors by distance from diaphragm location Are: Yellow (10.36 ft), Green (12 ft), Purple (13.64 ft)

Other data had repeating patterns which can be seen in Figure 29.

Figure 29

Open 20 ft Shock Tube Data of 4 Layered Sheet of Freezer Paper Diaphragm Burst at 49 psig

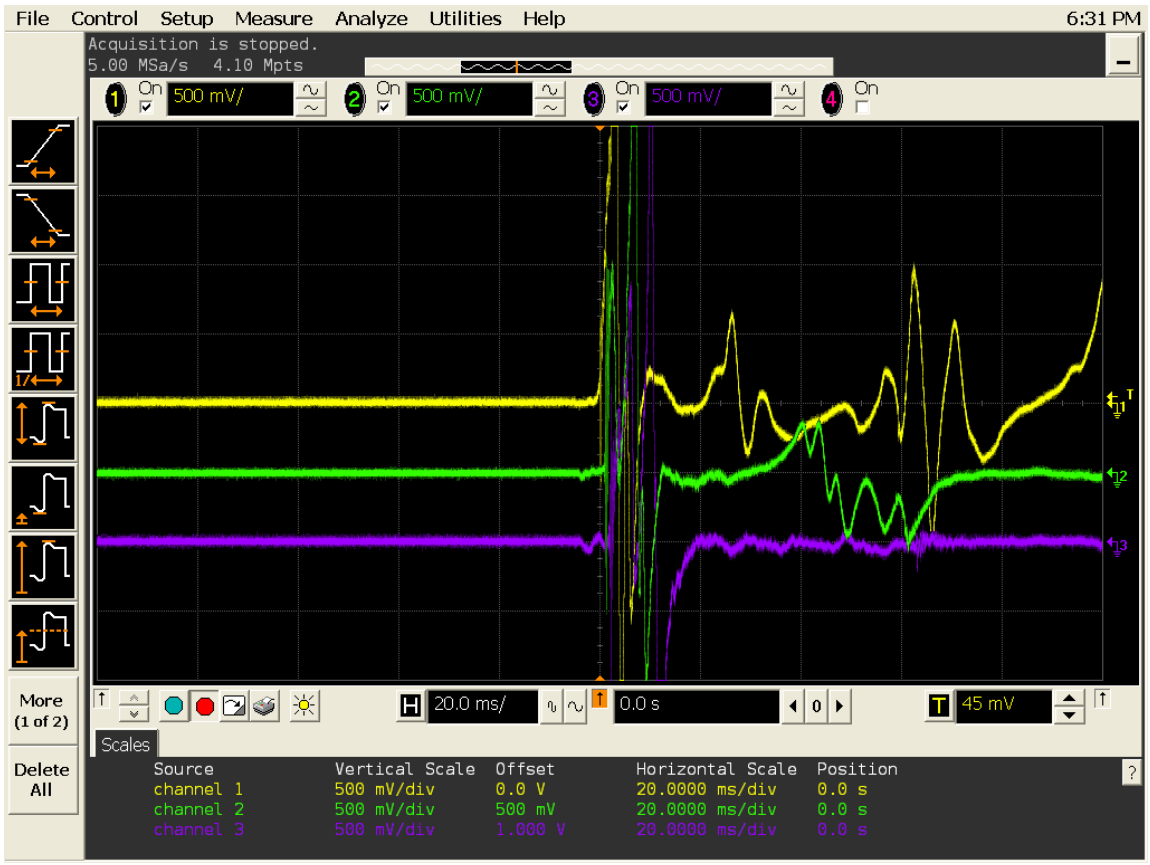

Note. Sensor colors by distance from diaphragm location are: Yellow (10.36 ft), Green (12 ft), Purple (13.64 ft).

This can be seen on one, two, or all three sensors and has no noticeable set time for continuation. This is probably an influence on from the paper as the overhead sheets do not give data as this.

Plotting velocities calculated from time-of-flight measurements collected at sensors 1 and 2 (Figure 30) helps us qualitatively understand the system behavior and how data may be better collected.

Figure 30

Graph of Open 20 ft Shock Tube for Varying Burst Pressures of Air into Air

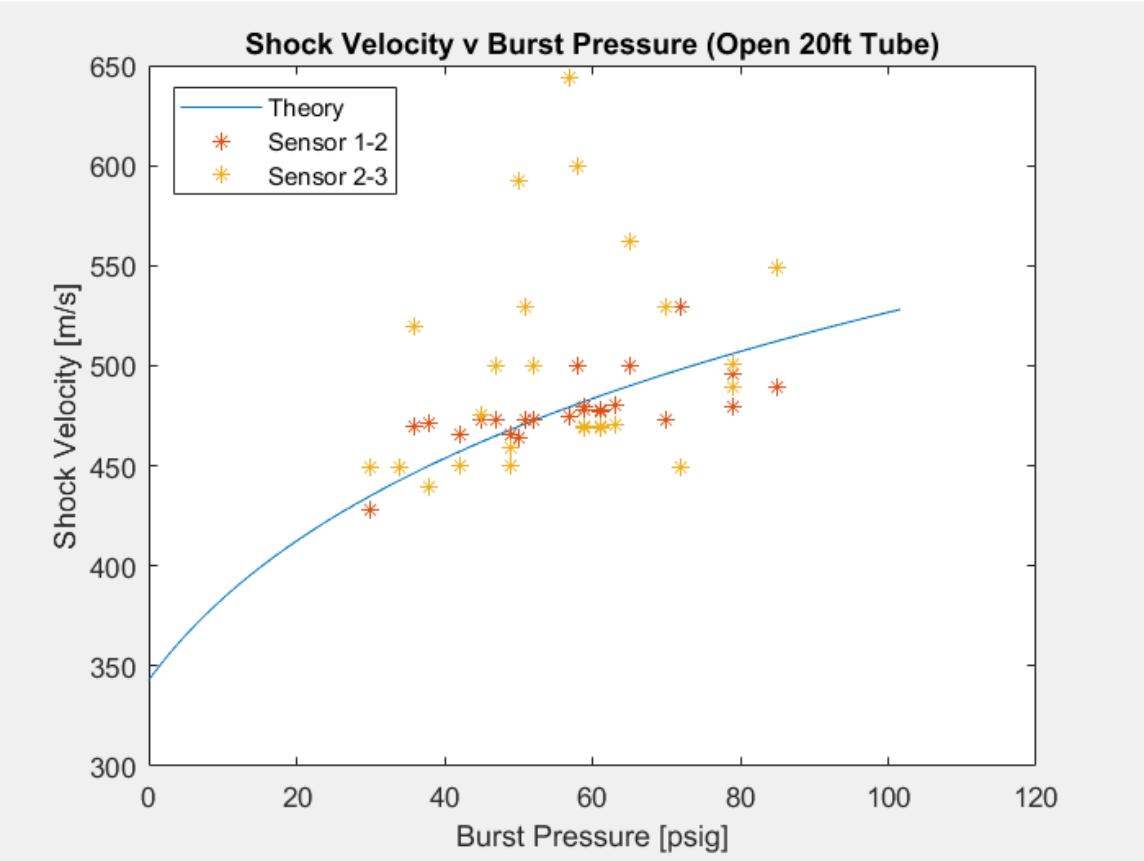

Note. Sensor displacements from diaphragm are: Sensor 1 at 10.36 ft, 2 at 12 ft, and 3 at 13.64 ft.

Some of the experimental values are close to the expected theoretical values, especially from sensors 1-2, but results are not convincing enough to say that what has been built works as intended. The data needs to be more precise before closing the shock tube. What was noticed was when zoomed in enough each shock wave passage gave a recognizable pattern to one another. There is a steep incline but then swoops down to a trough, whether smooth or converging to a point, which changes to another steep incline. After the incline

is where, as stated before, the voltage change gradually drops until zero. We then decided that the shock wave passage can be defined as the max trough of the waveforms.

The second trial of the open shock tube was conducted with each shock wave passage counted at the max trough. This gave us more reassurance as the results were closer to the theoretical than the first trial, as seen in Figure 31.

Figure 31

Second Trial Experimentation of Open 20 ft Shock Tube for Varying Burst Pressures of Air into Air

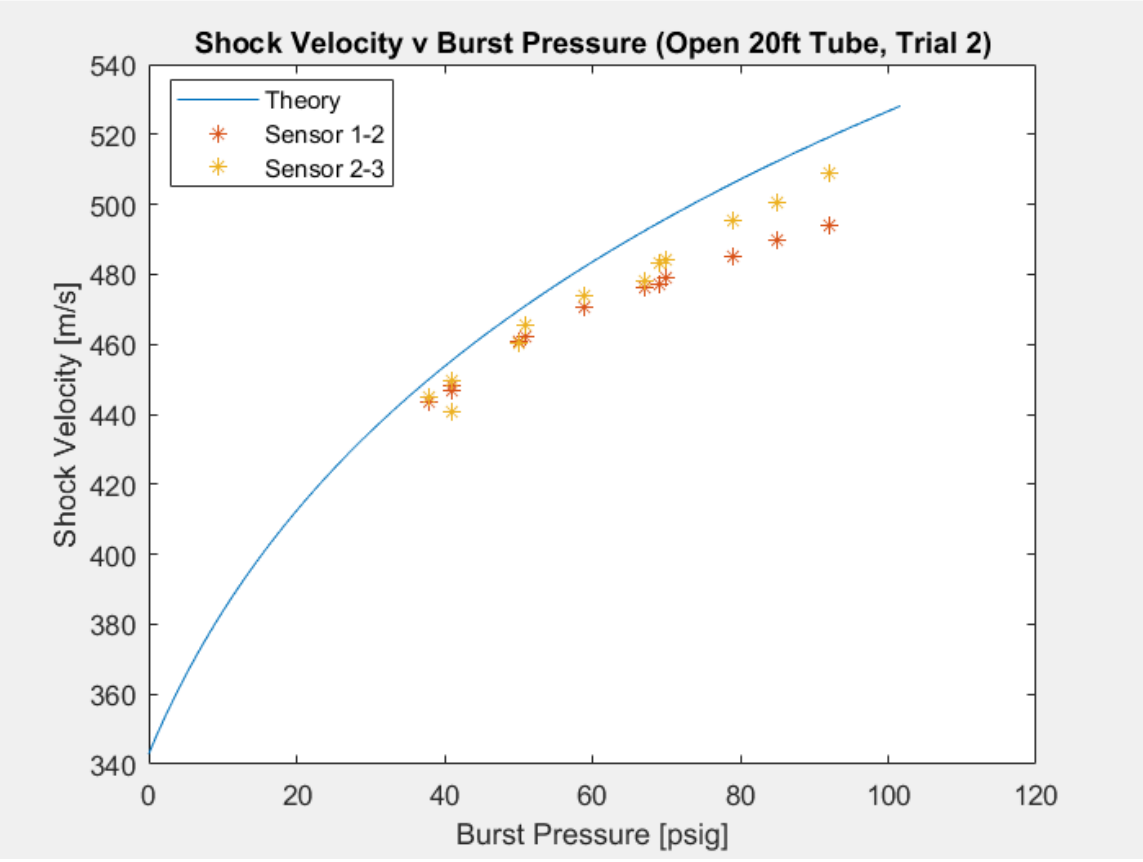

Note. Sensor displacements from diaphragm are: Sensor 1 at 10.36 ft, 2 at 12 ft, and 3 at 13.64 ft.

The deviation was outstandingly minimized as well. The shock wave seems to be accelerating at the last section of the tube, even more so at higher burst pressures, which would make sense since the waves are traveling at a higher maximum velocity.

Testing the Closed Shock Tube

Closing the End Section

Now that the open shock tube data has been verified, the shock tube is closed for comparing open and closed shock wave velocities and reflected shock wave velocities. The end section of the tube is a five-foot section with flanges on both sides, having a water jetted ⅜ inch aluminum with a tapped hole for the end wall sensor as seen in Figure 32 (b).

Figure 32

Detached End Section with Sensors Inserted Viewing the (a) Whole Section and (b) End Wall Section

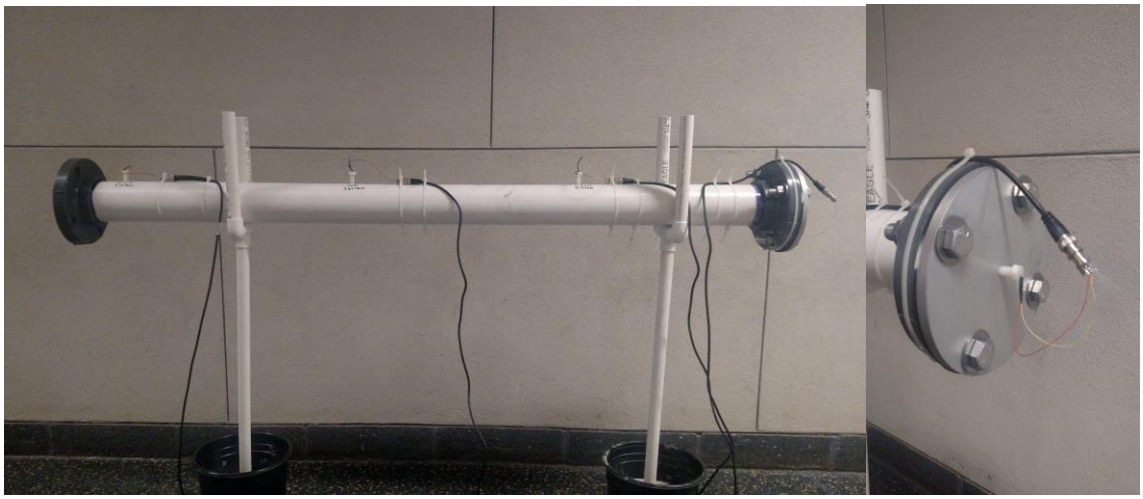

(a) (b)

With the end wall on, the shock tube, when fired, is substantially quieter since the energy from the rupture process remained inside of the sealed tube. One can hear a quickly decaying vibration frequency coming from the tube itself and support forks, but overall sound pressure level outside of the tube is diminished. Nevertheless, it is good to still wear ear protection in case something was to happen, or if anything is not sealed completely.

Closing the tube closed created more time for cleaning between each shot as the freezer paper diaphragms cause a slight mess after each shot. The steps between each shot were to open the shock tube at the diaphragm location to take out the material still sandwiched between the gaskets. While keeping that section open the end wall was removed by taking three bolts out while leaving one on so the sensor did not have to be removed. Enough wire was given to the sensor leads so this could be done without snapping any wires. The next step was to lift the driver side and point the open end towards the ground, so the diaphragm material would fall out. After placing the driver side back down, the rest of the tube was blown from the opening of the driven side. One good breath should be able to get the material out, but sometimes a few may be necessary. A couple shots from an air hose nozzle can easily get any material out. Closing the tube was the reverse of opening.

Testing the sensors in the closed shock tube gave us what we wanted, excluding the contact surface. Each shot was able to give the incident and reflected shock waves. The data even showed a response from the reflected shock wave, as seen in Figure 33.

Figure 33

Sensor Two at 12 ft from the Diaphragm's Visual Data of Shock Wave Passage Seen at 100 µs/div

Analyzing Closed Shock Tube Data

While observing the closed shock tube data, the end wall sensor experienced an abrupt spike in the signal but caused a negative trough as the other sensors did. Every time recorded for the spike resulted in a value roughly 20 or 30 m/s above the theoretical. It would make sense that the abrupt spike would be the sudden reflection of the shock wave but having an acceleration that would cause the data to be above theoretical was troubling. Therefore, the trough was still determined to the best of our ability for all the shock wave

passages. The results were on point, but the end wall slowed down drastically with recording at max troughs. Unlike the smooth troughs of the other sensors the end wall sensor's trough was rough, as seen in Figure 34.

Figure 34

End Wall Sensor Visual Data of Shock Reflection Seen at 100 µs/div

The other sensors give acceptable results. Looking at Figure 35, the recorded shock wave velocity tends to steadily decrease compared to what is expected from theory. This may be explained by physical reasons such as shock waves losing speed from energy dissipation into the walls or boundary layer effects. Nevertheless, these results are

remarkable for having a $5-dollar sensor assembly consisting of a 450 kHz piezoelectric sensor glued to a nylon screw.

Figure 35

Graph of Closed 20 ft Shock Tube for Varying Burst Pressures of Air into Air

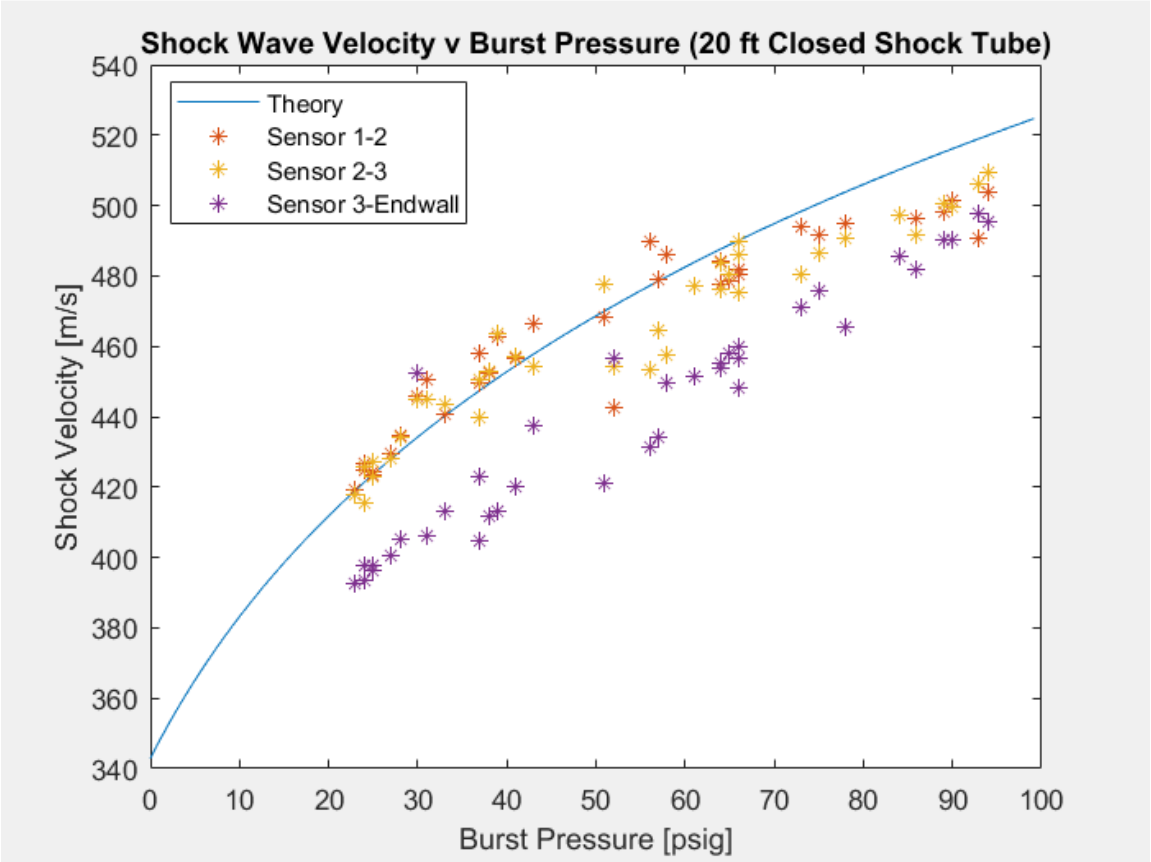

Note. Sensor displacements from diaphragm are: Sensor 1 at 10.36 ft, 2 at 12 ft, 3 at 13.64 ft, and end wall at 15 ft.

Comparing 15 and 20 ft Shock Tubes. The shock tube was condensed to 15 feet by taking one of the extension sections off to observe if there are any differences with acceleration from shock wave development. Figure 36 was graphed from the velocities calculated from sensors 1-2. Surprisingly there was no noticeable difference when

compared to each other. This could be a correction to the shock wave development length as stated before, the length calculated was not certain but more of an assumption.

Figure 36

Graph of Closed 15 and 20 ft Shock Tube for Varying Burst Pressures of Air into Air

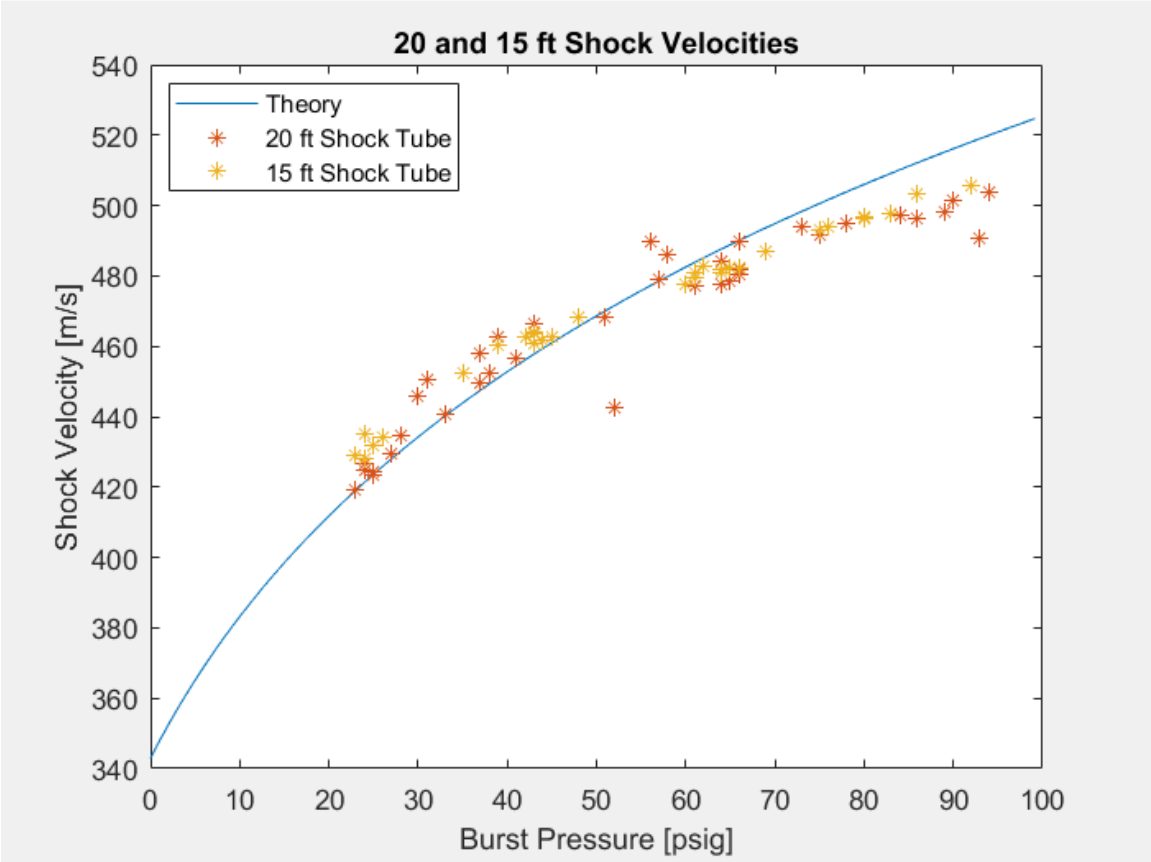

Note. Sensor displacements from diaphragm are: Sensor 1 at 10.36 ft, and 2 at 12 ft.

Argon into Air Shots. The next shots were done with diverse driver gases in the 20-foot shock tube. We wanted to make sure that if a different driver gas was used the experimental results would still hold up to theory. Argon was used since it was non-explosive, inexpensive, and heavier with a different specific heat capacity ratio. As seen in Figure 37, argon shocks were faster than expected, neglecting the velocity from sensor 3

to the end wall. Knowing the driver side gas was not pure argon, due to the presence of trace air, this is expected. The velocities follow the curve and experience the same pattern as the data from the 20-foot closed shock tube in Figure 35. There is a possibility that since argon is denser than air the driver side of the tube could have leftover argon from previous shots even after cleaning out the diaphragm material. This would make the expected shots more accurate compared to theory as the shots were made from low to high burst pressures when experimenting.

Figure 37

Graph of Closed 20 ft Shock Tube for Varying Burst Pressures of Argon into Air

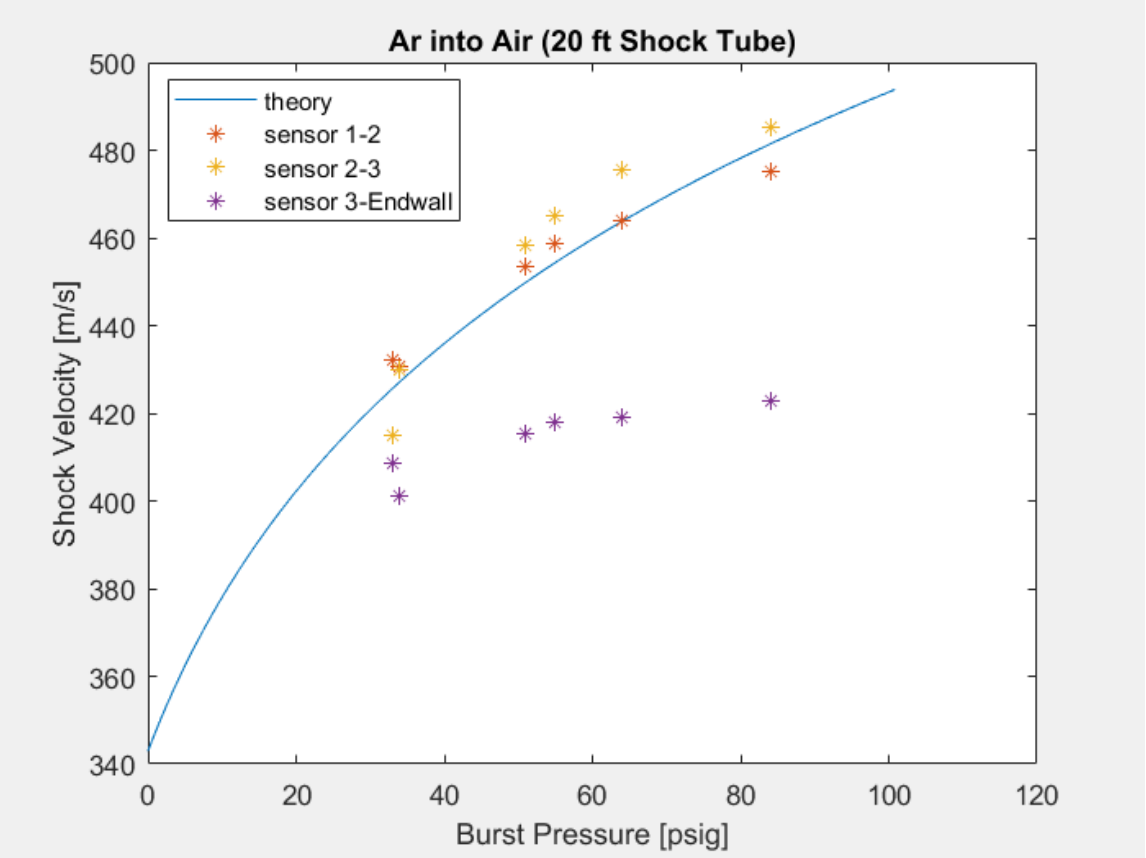

Note. Sensor displacements from diaphragm are: Sensor 1 at 10.36 ft, 2 at 12 ft, 3 at 13.64 ft, and end wall at 15 ft.

Helium into Air Shots. The next driver gas tested was helium. Fewer shots were conducted as helium is a rather expensive gas, so the price of each shot is rather costly. Three tests were done at lower burst pressures. Unfortunately, two shots happened to have the same burst pressure, so it's harder to see any curve pattern, but it is useful to compare any deviation. Figure 38 shows the data given for the three shots of helium into air. The graph shows an increasing velocity for higher bursting pressures, but the values are lower than expected. Like the argon shots the helium was mixed with air in the driver section, so

the density of the gas mixture was heavier than pure helium. Even though helium is lighter than argon, some helium could still be inside the driver side after each shot, making the mixture purer in helium than the first shot. It is great that the sensors are indeed working at the velocities that helium traveled at as these shots were the same speed as the highest shots seen with air into air. It would be good to examine what would happen if the diaphragm burst at around 90 to 100 psig to witness if the sensors would be able to send a signal fast enough for the oscilloscope to display a sharp enough peak for recording shock speed at maximum velocity.

Figure 38

Graph of Closed 20 ft Shock Tube for Varying Burst Pressures of Helium into Air

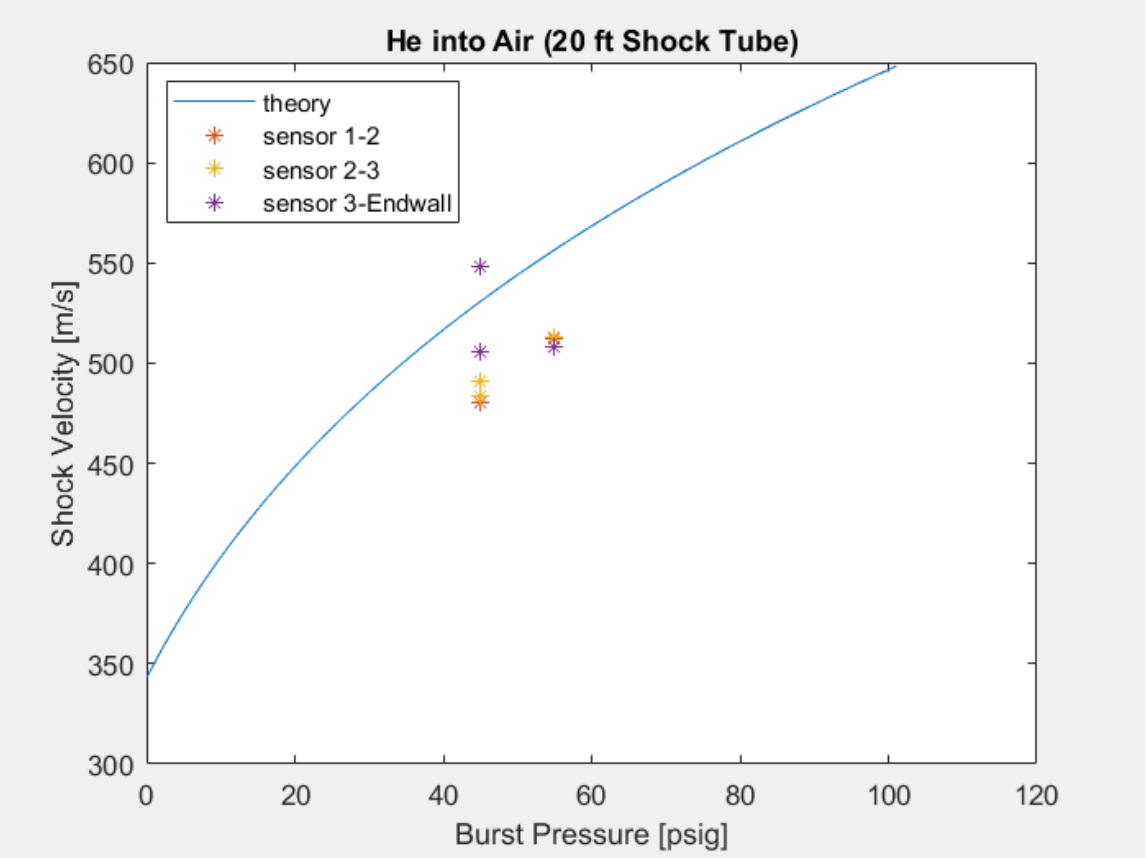

Note. Sensor displacements from diaphragm are: Sensor 1 at 10.36 ft, 2 at 12 ft, 3 at 13.64 ft, and end wall at 15 ft.

Measuring Shock Passage at Max Crest. Since measuring max trough for shock wave passage times did not always appear satisfactory, the peaks of the max crest were tested in the 20 ft closed shock tube. Since piezoelectric sensors seem to have a spike with a not much slower decay, it was thought that the sensor sends a positive voltage signal when compressed and overshoots a negative signal while expanding again when going back to equilibrium. Shots were tested three times instead of five times for each number of layered shots. Compared to the closed 20 ft shock tube measured at max trough, the max

crest measurements gave a much cleaner graph, minus the one outlier shot, as seen in Figure 39. This is great news considering that the deviation shrunk even more, and the shock velocities follow the curve more distinctly. One thing to point out is that the shock passage from sensor 3-Endwall follows the theoretical curve the best out of the other sensors and stays about the same distance away from the theoretical curve for each shot. The data here is very convincing that the sensors work how they are intended to, and it proves that our experiment fits theoretical calculations for the incident shock wave velocity.

Figure 39

Graph of Closed 20 ft Shock Tube for Varying Burst Pressures of Helium into Air

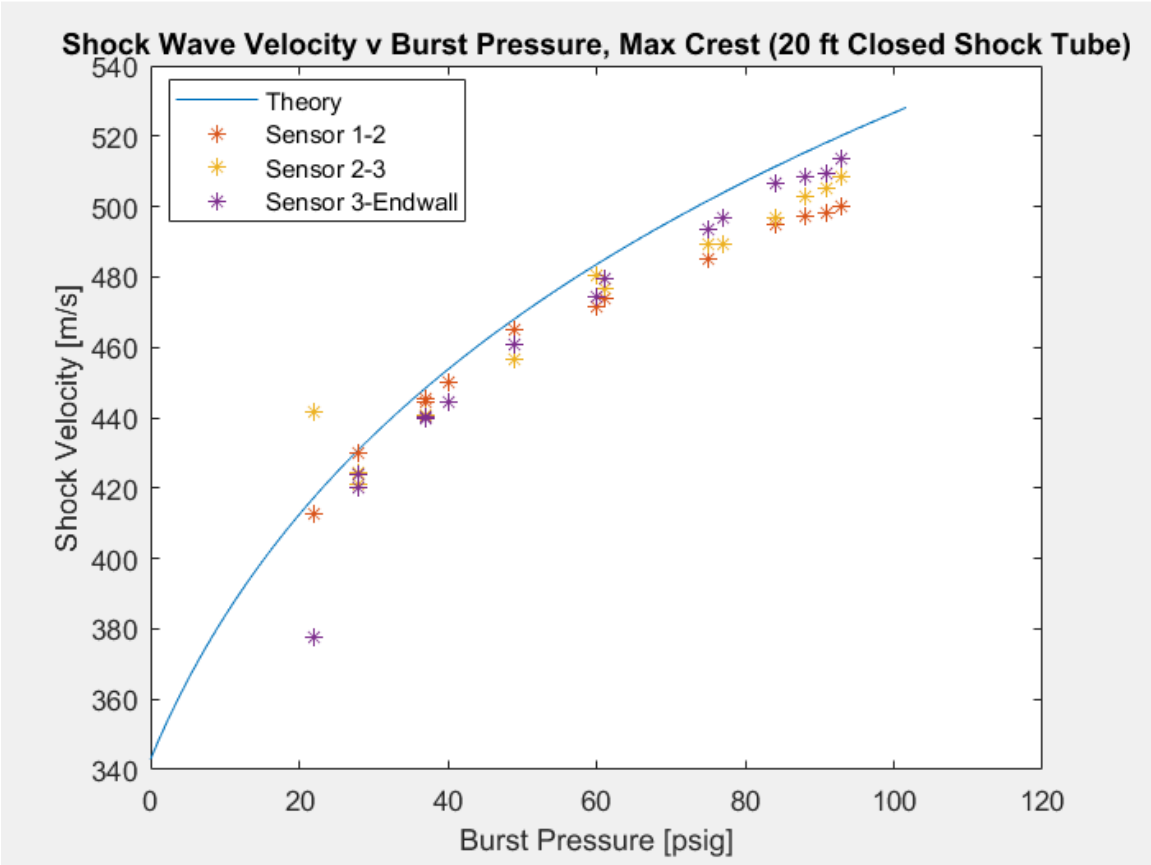

Note. Incident shock wave passage times measured at max crest. Sensor displacements from diaphragm are: Sensor 1 at 10.36 ft, 2 at 12 ft, 3 at 13.64 ft, and end wall at 15 ft.

Reflected Shocks. The next data to show is the reflected shock wave. Velocities from the reflected shock wave appear slower than theoretically predicted as they lose energy from energy transmitting into the walls and incoming pressure waves. Figure 40 plot isn't as pleasing to the eye as the incident shock front, but the data didn't diverge too far from theory. The lower burst pressures were able to keep values closer to theory, but as the burst pressures increase, the divergence of the expected values go farther from it. The passages of the reflected shock waves weren't as easy to determine as the incident passages.

One can see that the reflected passage from sensor 3 is more difficult to figure out than sensors 2 and 1.

Figure 40

Reflected Shock Wave Velocities of Closed Shock Tube with Shock Passage Times Recorded at Max Crest

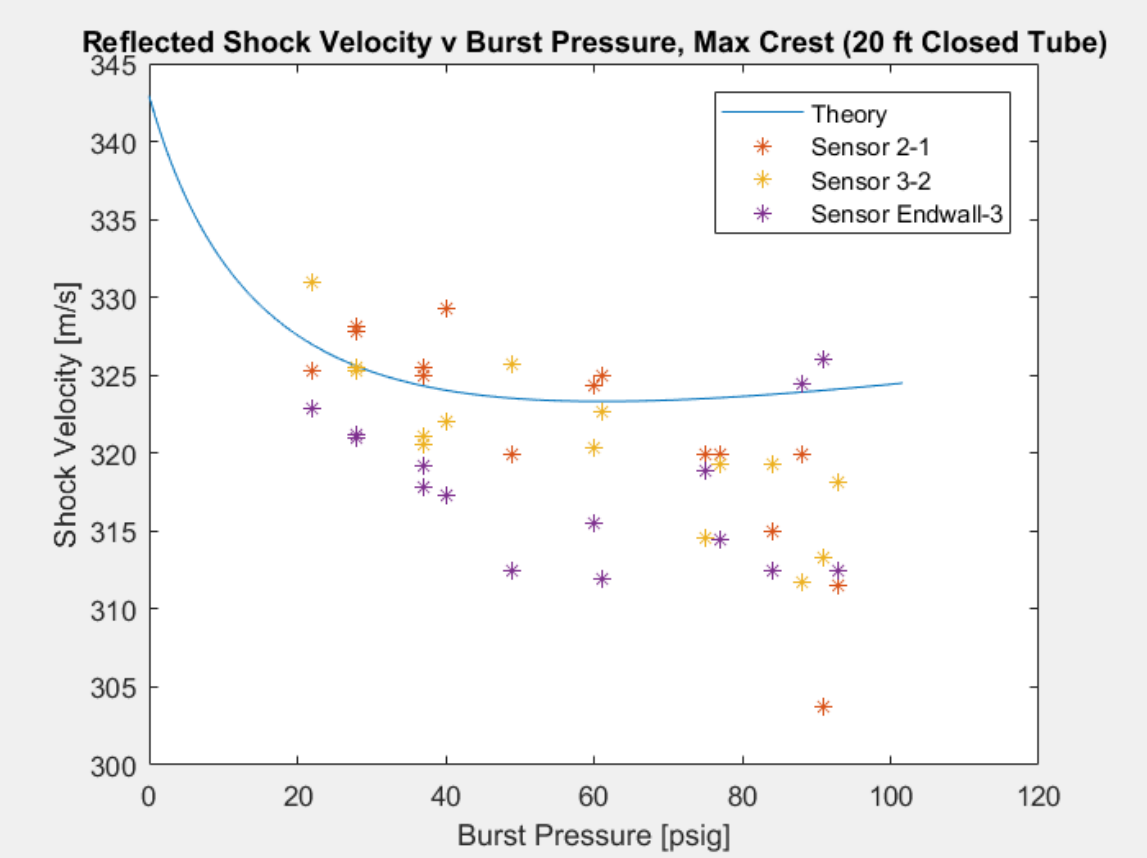

The height of sensor 3 from the shock tube inner walls was adjusted, but the same results came from the sensor. So, the first noticeable disturbance that wasn't an oscillation was recorded to be a passage. Sensor 3 is harder to see, but the passage disturbance is at the middle of the screen on Figure 41 a. The distances were divided by the theoretical

velocities to find the time it would take to get to sensor 3, and the recorded times were right about where the first disturbances were noticed.

Figure 41

Zoomed-In Reflected Shock Wave Passages

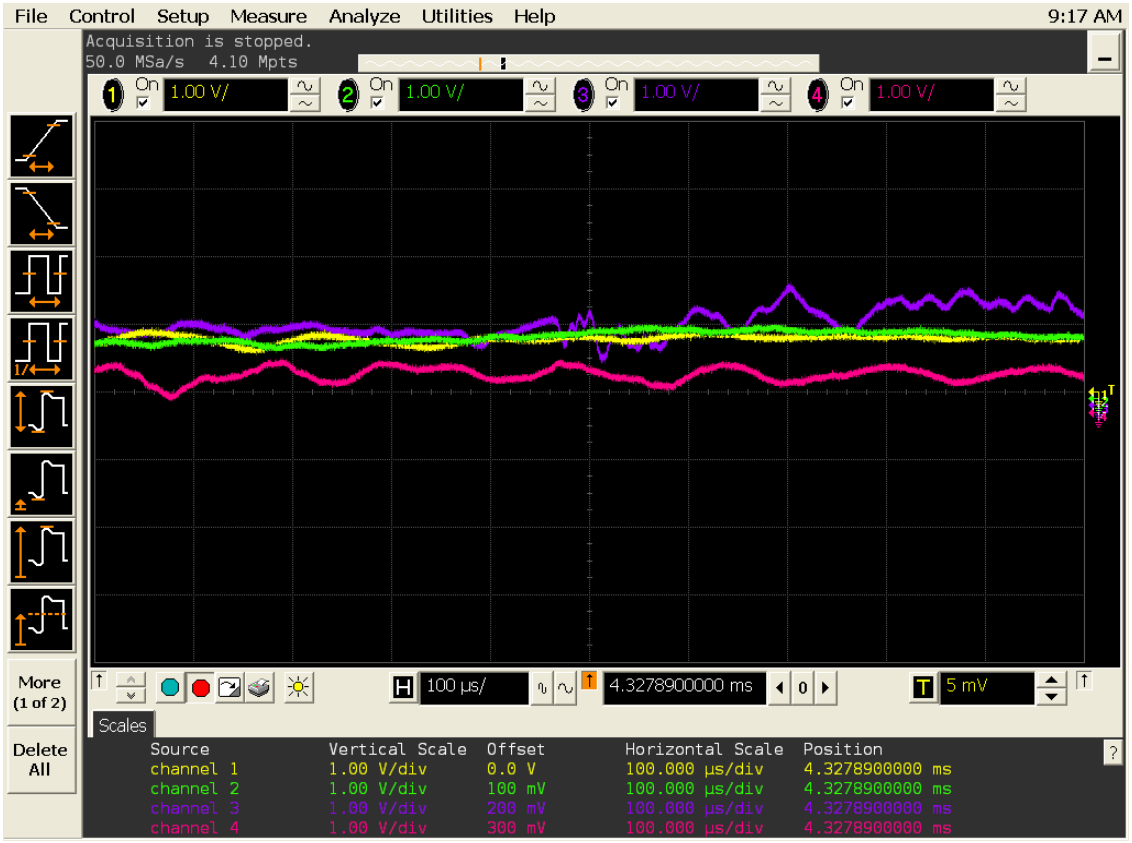

(a)

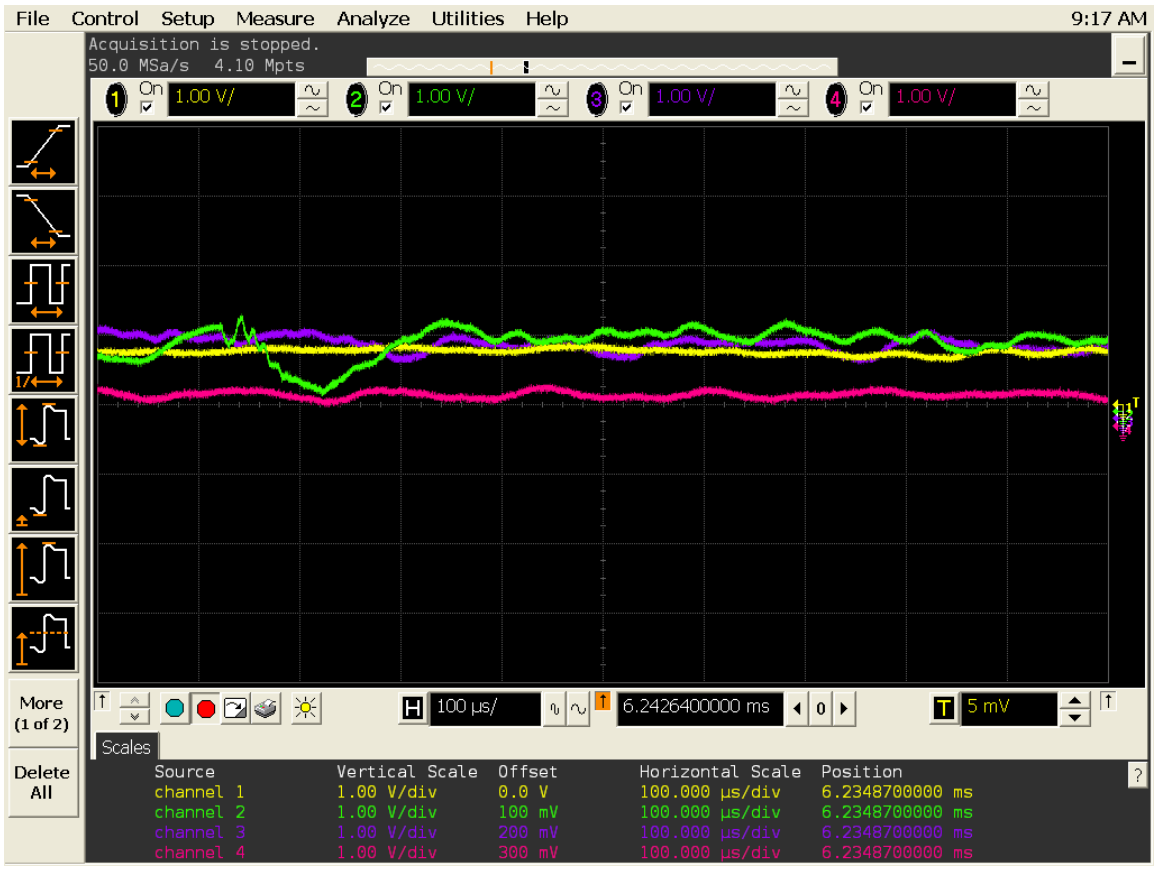
File Control Setup Measure Analyze Utilities Help 9:17 AM
Acquisition is stopped.
50.0 MSa/s 4.10 Mpts
1 On 1.00 V/
2 On 1.00 V/
3 On 1.00 V/
4 On 1.00 V/
More (1 of 2)
Delete All
100 µs/
6.2426400000 ms
0
5 mV
Scales
Source Vertical Scale Offset Horizontal Scale Position
channel 1 1.00 V/div 0.0 V 100.000 µs/div 6.2348700000 ms
channel 2 1.00 V/div 100 mV 100.000 µs/div 6.2348700000 ms
channel 3 1.00 V/div 200 mV 100.000 µs/div 6.2348700000 ms
channel 4 1.00 V/div 300 mV 100.000 µs/div 6.2348700000 ms

(b)

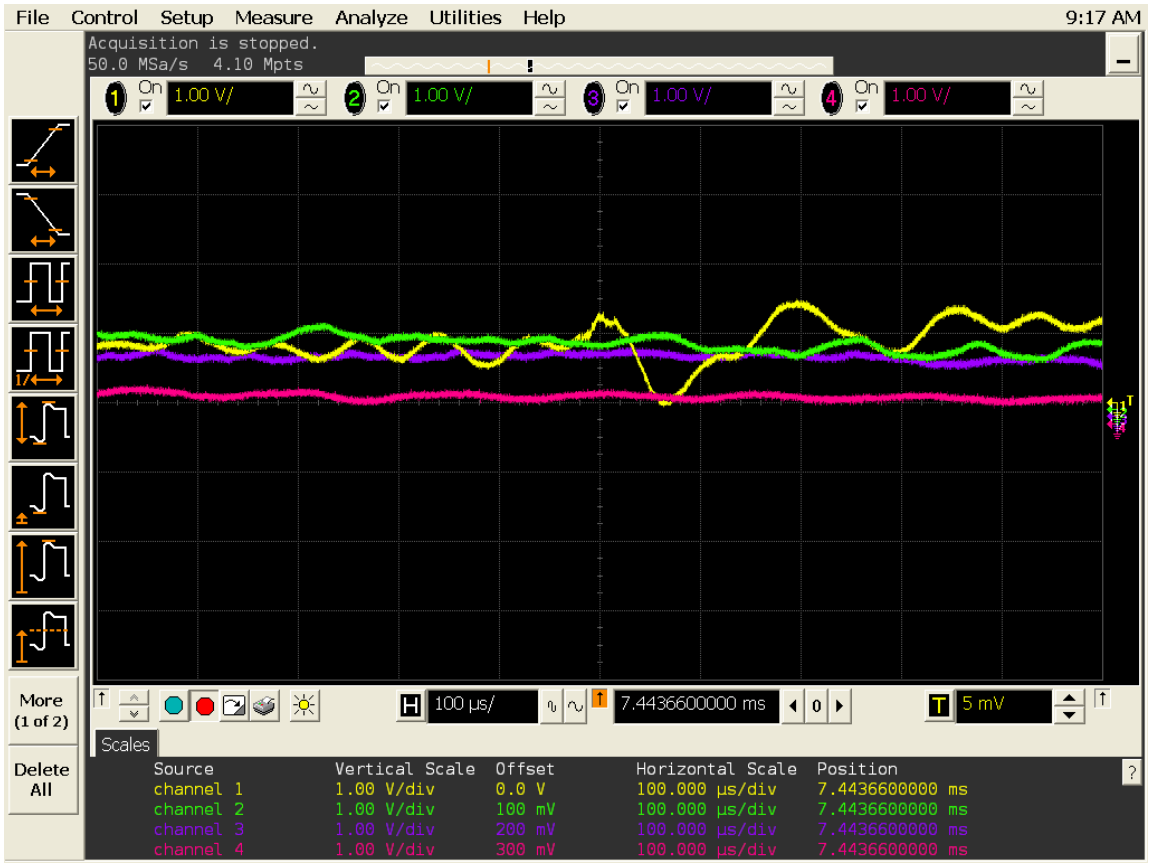

(c)

Note. (a) Sensor 3 (Purple) at 13.64 ft, (b) Sensor 2 (Green) at 12 ft, and (c) Sensor 1 (Yellow) at 10.36 ft shot from 1 overhead sheet diaphragm burst at 60 psig.

Aside from an inability to define passage of the contact surface, the sensors were able to prove themselves with theory, with very minimal error and great precision with a five-dollar sensor. We were able to interpret oscilloscope data with the help of the sensor having a fast-enough response and assuming the response from compressing it is most likely from the positive change in voltage. From the materials used, excluding the luxury oscilloscope, this project was able to show mostly what was desired in comparing experimental data to theory by using common items that can be found at a local hardware store and soldering together considerably inexpensive electronics connected to an

oscilloscope. If an institution desires to have a shock tube for non-explosive gases reaching velocities at supersonic speeds, it can now be done at around $500 USD or less.

Shock Tube Expenses

With all the materials that could possibly be ordered for our 20 ft single diaphragm PVC shock tube, the total came out to be $508.38. This includes compression fittings for the portholes for the extension sections, which was not used for this experiment. Many institutions will have some of these materials already which includes the quarter inch air hose, BNC cables, concrete, PVC, quick disconnect fittings (if desired over compression fittings), end wall material (if chosen to hand make or not purchase the blind flange from the McMaster-Carr website), and more. The total price is if someone or an institution has absolutely no parts readily available in constructing this tube. This price also does not include shipping and handling or any tools that may be needed. Some of these materials add to the expense of the total as they are only sold in packs or set lengths instead of individual parts, such as bolts, nuts, washers, nylon screws, piezoelectric sensors, etc. The final price can also vary depending on the discretion of materials bought as different businesses have different prices for their materials. So, the ultimate price of this shock tube can be under $500, but we want to make sure the developer has all the materials needed for our version of a shock tube.

Chapter 7

Future Work

The essential goal of this project has been achieved, but there remains more opportunity to progress the development of this shock tube platform. For one, the current shock tube is currently set up for the study of one-dimensional gas dynamics. One extension of the shock tube can be used to study to two-dimensional shock wave theory through oblique shocks formed as supersonic flow passes around wedge-, cone-, and/or obliquely shaped surfaces. This can consist of constructing the end test section with a square-shaped cross-sectional area, preferably using transparent material, and mounting a small, centrally located solid obstruction inside (e.g., a wedge). As our oscilloscope was set with a trigger sensor to start recording shock wave passage, the same concept can be used to trigger a fast-acting camera to take multiple images while high speed flow passes across the obstruction. An optical arrangement that takes advantage of the schlieren effect would be able to "see" the shock structure formed by the interaction of the flow with the obstruction. Using this setup, attached and bowed shock waves could be examined and compared to two-dimensional shock wave theory; for example, in testing the θ-β-M relationship[16] among wedge angle (θ), shock wave angle (β), and upstream Mach number (M) for wedge obstructions.

Another development may involve converting the current setup into a double diaphragm shock tube. This would create a buffer section, permitting better control pressures for diaphragm bursting. In the current setup, the manually operated valve letting gas into the driver section remains open a moment after the diaphragm bursts. Though the driver gas velocity is slower than the shock wave, the valve being opened can possibly

disturb some of the idealized physics assumed for the expansion waves. Having a double diaphragm will permit the valve at the end of the shock tube to be closed, permitting fast extraction of gas out of the buffer section This causes the first diaphragm between buffer and driver sections to fail. The driver gas will then enter the buffer section to burst the second diaphragm nearly equal to the initial driver section pressure.

Smaller future projects can include strengthening or protecting the wire leads of the sensors to make them less prone to accidental breaking, including moving or disassembling from the shock tube. This is especially important for the end wall sensor for the end wall's constant assembling and disassembling. Fortunately, with the current setup and precautions, the connection on the end wall sensor only broke once out of an estimated 200 or more shocks made for this project. Another small project can be changing the flange setup of the diaphragm to something that will last longer. The nut, bolt, and washer setup has proved itself fit for the project, but after so many screwing and unscrewing operations, the threads on at least one of the fastener sets became stripped (roughly 50 uses). It would be beneficial to find a more durable setup for repeated usage.

References

[1] A. G. Gaydon and I. R. Hurle, *The shock tube in high-temperature chemical physics* (no. Book, Whole). New York Book: Reinhold Pub. Corp, 1963.

[2] R. J. McMillan, "Shock tube investigation of pressure and ion sensors used in pulse detonation engine research," AIR FORCE INST OF TECH WRIGHT-PATTERSONAFB OH DEPT OF AERONAUTICS AND …2004.

[3] K. Yasunaga, H. Yamada, H. Oshita, K. Hattori, Y. Hidaka, and H. Curran, "Pyrolysis of n-pentane, n-hexane and n-heptane in a single pulse shock tube," *Combustion and Flame,* vol. 185, pp. 335-345, 2017.

[4] E. L. Petersen and R. K. Hanson, "Nonideal effects behind reflected shock waves in a high-pressure shock tube," *Shock Waves,* vol. 10, no. 6, pp. 405-420, 2001.

[5] S. M. Burke *et al.*, "An experimental and modeling study of propene oxidation. Part 2: Ignition delay time and flame speed measurements," *Combustion and Flame,* vol. 162, no. 2, pp. 296-314, 2015.

[6] J. H. Grinstead, M. C. Wilder, D. C. Reda, C. J. Cornelison, B. A. Cruden, and D. W. Bogdanoff, "Shock tube and ballistic range facilities at NASA ames research center," presented at the Aerothermodynamic Design, Review on Ground Testing and CFD, 29 Mar. - 1 Apr. 2010; Genese; Belgium, Mar 29, 2010, 2010.

[7] R. Mehta, "Numerical simulation of supersonic flow past reentry capsules," *Shock Waves,* vol. 15, no. 1, pp. 31-41, 2006.

[8] M. Sackmann *et al.*, "Shock-wave lithotripsy of gallbladder stones," *New England journal of medicine,* vol. 318, no. 7, pp. 393-397, 1988.

[9] S. M. Auls'chenko, V. P. Zamuraev, and A. P. Kalinina, "Nonlinear effects in the interaction of periodic pulsed energy supply and shock-wave structure during transonic streamlining of wing profiles," *Technical Physics Letters,* vol. 32, no. 1, pp. 3-5, 2006.

[10] T.-M. Jia, G.-X. Li, Y.-S. Yu, and Y.-J. Xu, "Propagation characteristics of induced shock waves generated by diesel spray under ultra-high injection pressure," *Fuel,* vol. 180, pp. 521-528, 2016.

[11] G. I. Kanel, S. V. Razorenov, and G. V. Garkushin, "Rate and temperature dependences of the yield stress of commercial titanium under conditions of shock-wave loading," *Journal of Applied Physics,* vol. 119, no. 18, p. 185903, 2016.

[12] M. Tavakol, M. Mahnama, and R. Naghdabadi, "Shock wave sintering of Al/SiC metal matrix nano-composites: A molecular dynamics study," *Computational Materials Science,* vol. 125, pp. 255-262, 2016.

[13] G. Zhang, Y. Z. Jin, T. Setoguchi, and H. D. Kim, "Study on drug powder acceleration in a micro shock tube," *Journal of Mechanical Science and Technology,* vol. 30, no. 9, pp. 4007-4013, 2016.

[14] S. Tang, F. Tesler, F. G. Marlasca, P. Levy, V. Dobrosavljevic, and M. Rozenberg, "Shock waves and commutation speed of memristors," *Physical Review X,* vol. 6, no. 1, p. 011028, 2016.

[15] P. Akbari and I. Agoos, "Two-Stage Wave Disk Engine Concept and Performance Prediction," 2017. Available: https://doi.org/10.4271/2017-01-2046

[16] J. D. ANDERSON, "Modern compressible flow, with historical perspective," McGraw-Hill0070016739, 1990.

[17] S. Prunty, *Introduction to Simple Shock Waves in Air: With Numerical Solutions Using Artificial Viscosity*. Springer Nature, 2021.

[18] E. Ninnemann *et al.*, "New insights into the shock tube ignition of H2/O2 at low to moderate temperatures using high-speed end-wall imaging," *Combustion and Flame,* vol. 187, pp. 11-21, 2018.

[19] D. R. White, "Influence of diaphragm opening time on shock-tube flows," *Journal of Fluid Mechanics,* vol. 4, no. 6, pp. 585-599, 1958.

[20] K. Alexandrino, M. U. Alzueta, and H. J. Curran, "An experimental and modeling study of the ignition of dimethyl carbonate in shock tubes and rapid compression machine," *Combustion and Flame,* vol. 188, pp. 212-226, 2018.

[21] P. J. Brown, "Shock Tube Experiments for the Determination of Petrophysical Parameters," Dissertation/Thesis, ProQuest Dissertations Publishing, 2002.

[22] B. J. Cantwell, "Fundamentals of Compressible Flow," in *Fundamentals of Compressible Flow*: Stanford University, 2018.

[23] S. Downes, A. Knott, and I. Robinson, "Towards a shock tube method for the dynamic calibration of pressure sensors," *PHILOSOPHICAL TRANSACTIONS OF THE ROYAL SOCIETY A-MATHEMATICAL PHYSICAL AND ENGINEERING SCIENCES,* vol. 372, no. 2023, pp. 20130299-20130299, 2014.

[24] A. Fridlyand, P. T. Lynch, R. S. Tranter, and K. Brezinsky, "Single pulse shock tube study of allyl radical recombination," *Journal of Physical Chemistry A,* vol. 117, no. 23, pp. 4762-4776, 2013.

[25] S. Gowdagiri, "Fuel Autoignition Variability: Shock Tube Measurements, a Reduced Kinetic Model and Diesel Engine Studies," Dissertation/Thesis, ProQuest Dissertations Publishing, 2014.

[26] C. H. Group. *T5 Reflected Shock Tunnel*. Available: http://shepherd.caltech.edu/T5/facilities/T5/T5.html

[27] P. R. Group. *Aerosol Shock Tube Facility*. Available: https://petersengroup.tamu.edu/facilities/aerosolshocktubefacility.html

[28] P. R. Group. *High Pressure Shock Tube*. Available: https://petersengroup.tamu.edu/facilities/highpressureshocktubefacility.html

[29] S. Jouzdani, "Shock Tube and Mid-IR Laser Absorption Study of Combustion Kinetics," Dissertation/Thesis, ProQuest Dissertations Publishing, 2018.

[30] Y. Mao *et al.*, "An experimental and kinetic modeling study of n-butylcyclohexane over low-to-high temperature ranges," *Combustion and Flame,* vol. 206, pp. 83-97, 2019.

[31] S. R. Nanda, S. Agarwal, V. Kulkarni, and N. Sahoo, "Shock tube as an impulsive application device," *International Journal of Aerospace Engineering,* vol. 2017, pp. 1-12, 2017.

[32] R. Sivaramakrishnan, J. V. Michael, L. B. Harding, and S. J. Klippenstein, "Shock tube explorations of roaming radical mechanisms: The decompositions of isobutane and neopentane," *Journal of Physical Chemistry A,* vol. 116, no. 24, pp. 5981-5989, 2012.

[33] X. Yang, A. W. Jasper, J. H. Kiefer, and R. S. Tranter, "The dissociation of diacetyl: A shock tube and theoretical study," *Journal of Physical Chemistry A,* vol. 113, no. 29, pp. 8318-8326, 2009.

[34] H. Plastics. *PVC Schedule 40 Pressure/DWV Pipe (drain, waste and vent)*. Available: http://www.heritageplastics.com/pvc-water-plumbing-pipe-east/pvc-schedule-40-pressure-dwv-pipe/

[35] M. S. Downey, T. J. Cloete, and A. D. B. Yates, "A rapid opening sleeve valve for a diaphragmless shock tube," *Shock Waves,* vol. 21, no. 4, pp. 315-319, 2011.

[36] P. T. Lynch, "Note: An improved solenoid driver valve for miniature shock tubes," *Review of Scientific Instruments,* Article vol. 87, no. 5, pp. 056110-1-056110-3, 2016.

[37] R. Mejia-Alvarez, B. Wilson, M. C. Leftwich, A. A. Martinez, and K. P. Prestridge, "Design of a fast diaphragmless shock tube driver," *Shock Waves,* vol. 25, no. 6, pp. 635-650, 2015.

[38] R. S. Tranter and P. T. Lynch, "A miniature high repetition rate shock tube," *Review of Scientific Instruments,* Article vol. 84, no. 9, pp. 094102-094102-11, 2013.

[39] Jeremy. *Details for the SGTC Supah-Valve*. Available: https://www.spudtech.com/detail.asp?id=39

[40] Jeremy. *Build Your Own Launcher*. Available: https://www.spudtech.com/content.asp?id=5

[41] 3M. *3M Transparency Film: Frequently Asked Questions*. Available: http://multimedia.3m.com/mws/media/377903O/3mtm-transparency-film-general-faqs.pdf

Appendix A

Manufacturing Instructions

Support Forks (Makes 8)

1. Wear appropriate personal protective equipment (gloves, dust mask, safety glasses)
2. Cut ¾ inch PVC pipe to eight 27-inch lengths. These are "support tubes" as indicated below.
3. Cover holes in flowerpots with waterproof material, preferably plastic, and tape material to the inside walls of the flowerpots.
4. Place concrete bag into mixing tub and slice bag open to pour while inside the tub to avoid spilling and any unnecessary airborne dust.
5. Add water little by little at a time (about 1-2 liters each time) while mixing with a bucket on one side of the tub to mix dry concrete evenly. Mix all the concrete evenly with each addition of water to ensure that the mixture does not become soupy. A crumbly mixture means that the concrete is too dry. A good mixture will be somewhere in the middle and stronger.
6. Using a shovel, scoop the concrete into four pots until full, and repeat steps 4 and 5 when necessary
7. Using a metal rod, stab the concrete in the pots multiple times to ensure enough air has escaped the mixture.
8. Place a support tube in each pot.
9. Repeat steps 6-8 for four additional pots.
10. Place four pots in a row.

11. Grab any unused ¾ inch pipe and couplings as needed and make two lengths of pipe long enough to extend past the row of pots. Place the pipes parallel and on top of the row of pots with one pipe on each side of the supports. Zip tie the two pipes together between each pot and on each end that extends past the pots as they will clamp the support pipes while the cement dries.

12. Position the supports so they are perpendicular to the ground. Use a level if needed.

13. Repeat steps 11 and 12 for the other four pots.

14. Let the concrete cure for 24 hours.

15. While the concrete is curing, cut more ¾ inch PVC into sixteen, 1¼ inch lengths.

16. For each of the ¾ inch 90-degree tee fittings, cut ¼ inch off each side of the tee, not including the perpendicular opening.

17. For the ¾ inch 90-degree elbow fittings, cut ¼ inch off one opening.

18. Cut sixteen pieces of the ¾ inch PVC into uniform (at least) 5-inch lengths.

19. Using the PVC primer and cement, join two of the 1¼ inch lengths of ¾ inch PVC to the cut openings of the tee fittings. After joining, use the primer and cement to join two of the 90-degree elbows onto the stubs protruding from the tee; be sure to join the sides of the elbow that were trimmed in step 17. Then join two of the 5+ inch lengths of PVC to the tee/elbow assembly. Repeat 8 times. These are “fork assemblies,” as indicated below.

20. Once the concrete has fully cured, join the fork assemblies to the support tube/flowerpot assemblies to complete the full support fork assembly.

High Pressure Fill Assembly (Driver Section)

1. Take a 10-foot 3-inch PVC and cut it in half across its diameter. (The other half will be used for end section).

2. Use PVC cement and primer to join a 3-inch flange with one end of the five-foot section. **When joining flanges with pipe make sure the holes of the flanges on any one section are aligned with each other on each side of the section and indicate what direction on the pipe faces up so machining and combining sections are done smoothly.**

3. Use the cement and primer to join the PVC reducing bushing to the other end of the section.

4. Wrap Teflon tape on the brass tee fitting threads and screw the tee into the ball valve port.

5. Wrap Teflon tape on the pressure relief valve threads and screw the valve into the perpendicular section of the tee.

6. Wrap Teflon tape on the pressure gauge damper threads and screw the damper into the tee.

7. Wrap Teflon tape on the male to male pipe adapter threads and screw the adapter into the ball valve.

8. Wrap Teflon tape on the plastic 1 inch to ¼ inch reducing fitting threads and screw the adapter into the ball valve.

9. Wrap Teflon tape around the valve assembly threads and screw the assembly into the threads in the reducer already attached to the shock tube in step 3.

10. Connect the ¼ inch hose to the compression fitting and wrap Teflon tape around the compression fitting threads. Screw the threads into the valve reducing fitting.

11. Attach the other end of the hose to the driver gas source.

12. Connect the high-pressure assembly to the extension assembly using nut/bolt fasteners.

Piezo Sensor Assembly

1. Drill a hole with the 3/32 drill bit into a nylon screw near the edge of the face opposite of the head where the piezoelectric sensor will sit. Drill through both sides since the drill bit is not long enough to go through one side. This process works best if access to milling machine is available. If too long, nylon screws can be shortened.

2. Use the wire stripper to strip about 3/16 inches of insulation off the piezoelectric sensor leads. (You can also very carefully use wire cutters as a stripping tool by almost completely closing the cutters just enough to cut through the insulation and pull to remove enough insulation for soldering.)

3. Carefully thread the sensor leads into the holes of the screw from the side opposite of the head and use the super glue to place the soldered side of the sensor down to the bottom of the nylon screw.

4. Cut 6 to 6½ inches of the red and black 28-gauge wires and strip about 3/16 inches of insulation on each side.

5. Attach the BNC solder connector to one end of a BNC cable and sand the terminals to remove any coating that may prevent poor electrical connection when joined.

6. Bend and fold one stripped end of the red and black wire to increase contact when soldering to the center (positive) terminal of the BNC solder connector. Solder these wire ends to the connector.

7. Cut shrink wrap into two half inch pieces and slide them over the red and black wires.

8. Bend and fold the other stripped end of the wires and the sensor wires together so they are hooked to each other and solder them together. Slip the shrink wrap over the exposed wire leads from the piezoelectric sensor and heat them to seal it. This will negate any possible shortage between the leads.

9. Use two cable ties to strap down the end of the BNC to keep it from moving. The sensor should only be free to move. Determine how many turns until the piezoelectric sensor is flush with the walls inside the tube, and pre-twist in the counterclockwise the same amount of turns to have the sensor leads untwisted when screwed in. Now screw in the piezo sensor and adjust accordingly until the sensor is flush with the inside walls.

Extension Sections

1. Take a 10-foot 3-inch PVC and cut it in half across the tube diameter.

2. Use PVC cement and primer to join a 3-inch flange with one end of the five-foot section.

3. Use PVC cement and primer to join a 3-inch flange with the other end of the five-foot section. **When joining flanges with pipe make sure the holes of the flanges on any one section are aligned with each other on each side of the section and indicate what direction on the pipe faces up so machining and combining sections are done smoothly**

4. Drill 7/16-inch holes 10 cm from the openings on one or both ends at the top of the pipe for port placement, if desired. The 10 cm spacing helps the holes not be too close to the flange when disassembling the shock tube.

5. Create threads in each hole from the ¼ npt-18 tap if portholes were cut.

6. Drill 5/16-inch holes 10 cm where desired, if desired, at the top of the pipe for sensor placement.

7. Create threads in each hole from the ⅜-16 tap if sensor holes were cut.

8. Connect the pipe to the rest of the shock tube using a bolt, washer, flange, gasket, flange, washer, nut configuration for each bolt hole when joining sections on each side.

9. If sections have tapped holes, fill holes with sensor assemblies, nylon screws with Teflon tape, compression fittings with Teflon tape, or any combination to seal the inside of the tube.

10. Repeat all steps for as many sections as desired.

End Section

1. Use the 3-inch diameter, 5-foot long section remaining after construction of the high pressure (driver) section

2. Use PVC cement and primer to join a 3-inch flange with one end of the five-foot section.

3. Use PVC cement and primer to join a 3-inch flange (if constructing closed shock tube) with the other end of the five-foot section. If constructing DIY end wall, use same instructions from steps 5-6 with your end wall. Allow 24 hours for the cement to cure before putting under pressure. **When joining flanges with pipe make sure the holes of the flanges on any one section are aligned with each other on each side of the section and indicate what direction on the pipe faces up so machining and combining sections are done smoothly**

4. On the side that will be connected to the extension section, mark a dot at 2 feet where the tube will sit upright from the flange. Mark a dot 0.5 meters ahead and behind

this 2-foot mark. At each mark, drill a hole using the 5/16-inch drill bit. After drilling, tap the holes with the ⅜-16 drill tap. If using a spigot connector with cap, first fill in the square hole with epoxy until it is flush with the rest of the cap's inside wall.

5. Grab the blind flange (or whichever end wall you are using) and mark a hole at the center of it. Drill a 5/16 hole at the location and tap a ⅜-16 thread. Use a nylon screw to determine how many turns it takes to have the piezoelectric sensor flush with the blind flange and PVC walls.

6. Bolt the blind flange to the end of the section and end section to the extension section making sure to sandwich the gasket between the flanges. When joining any section together, make sure to have a bolt, washer, flange, gasket, flange, washer, nut configuration. **If using a thin end wall flange, have the bolts face the shock tube for personal safety** (To help with calculations, get tape and mark hole location distances from the diaphragm location.)

7. Attach the sensors by using the instructions in the piezo sensor assembly section step 9. For the end wall sensor make sure enough cable and wire is free when having the flange hanging on one bolt while cleaning out the tube. This will give no tension on the wires and will keep them from snapping. If using a spigot connector with cap, either unscrew the sensor before unscrewing the cap, or find a surface to place the connected cap on.

Appendix B

Bill of Materials (20 ft Shock Tube)

Shock Tube Support Forks

1. 4x ($3.10/each) 60 lb. concrete bag - Home Depot SKU: 929514
2. 3x ($2.85/10 ft) ¾ inch schedule 40 PVC - Home Depot SKU: 136293
3. 16x ($0.59/each) 90-degree ¾ inch elbow fitting - Home Depot SKU: 187976
4. 8x ($0.59/each) ¾ inch schedule 40 tee fitting - Home Depot SKU: 187917
5. 1x ($9.17/each) PVC purple primer clear cement pack (for whole project) - Home Depot SKU: 462620
6. 8x ($2.47/each) Black plastic flowerpot - Home Depot SKU: 232000

Total: $64.04

High Pressure (Driver) Fill Assembly

1. 1x ($18.28/each) 10 ft 3-inch schedule 40 PVC (use other 5 feet for end section) - Home Depot SKU: 193860
2. 1x ($16.32/each) 3-inch Schedule 80 PVC flange - McMaster-Carr PN: 4881K218
3. 1x ($33.11/each) Ball valve - McMaster-Carr PN: 4085T23
4. 1x ($20.90/each) Pressure gauge - McMaster-Carr PN: 3846K211
5. 1x ($9.52/each) Pressure gauge vibration damper - McMaster-Carr PN:3820K23
6. 1x ($5.26/each) Pop safety valve McMaster-Carr PN: 48435K72
7. 1x ($4.90/each) Brass tee fitting - McMaster-Carr PN: 50785K222
8. 1x ($3.04/each) Compression fitting - McMaster-Carr PN: 50915K315
9. 2x ($3.78/each) Gasket - McMaster-Carr PN: 1082N15

10. 1x ($1.68/each) Valve reducing adapter - McMaster-Carr PN: 4880K672

11. 1x ($1.68/each) 3-inch PVC coupling - Home Depot SKU: 189030

12. 1x ($3.23/each) Reducing bushing - McMaster-Carr PN: 4880K222

13. 1x ($7.32/pack of 25) hex nuts (for whole project) - McMaster-Carr PN: 95505A607

14. 2x ($6.07/pack of 25) washers (for whole project) - McMaster-Carr PN: 92141A035

15. 2x ($12.13/pack of 10) bolts (for whole project) - McMaster-Carr PN: 91247A806

16. 1x ($8.00/50 ft length) ¼ inch air hose (for whole project) - McMaster-Carr PN: 5233K52

Total: $177.20

Piezo Sensor Assemblies

1. 1x ($29.00/pack of 10 + $9.95 flat rate shipping) Piezo sensors – Steiner & Martins, Inc. (Steminc) PN: SMD05T04R111WL

2. 1x ($7.29/pack of 25) Nylon screws - McMaster-Carr PN: 91244A624

3. 1x ($2.98/each) Super glue - Home Depot SKU: 686685

4. 4x ($6.14/each) BNC cable - McMaster-Carr PN: 6641T11

5. 4x ($6.30/each) BNC solder connector - DigiKey PN: 991-1036-ND

6. 1x ($2.99/pack of 100) Cable ties - Harbor Freight SKU: 34636

7. 1x ($1.53/each) Teflon tape - Home Depot SKU: 788287

8. 1x ($2.68/25 ft) Red 28-gauge wire - McMaster-Carr PN: 8054T31

9. 1x ($2.68/25 ft) Black 28-gauge wire - McMaster-Carr PN: 8054T31

10. 1x ($3.03/pack of 5 ½ ft lengths) Heat shrink tubing - McMaster-Carr PN: 7496K83

Total: $111.89

Standard Tools and Personal Protection Equipment (If Not Already Owned)

1. 1x ($5.97/each) Concrete mixing tub - Home Depot SKU: 535443
2. 1x Stirring rod for concrete (you can use anything)
3. 1x ($9.97/each) Shovel 765236
4. 1x ($5.47/each) Hacksaw - Home Depot SKU: 1000032953
5. 1x ($19.97/each) Soldering kit with gun, solder, and tips - Home Depot SKU: 1000011092
6. 1x or more ($1.98/each) Safety glasses - Home Depot PN: MCSCRWBK110
7. 1x or more ($12.59/each) Earmuffs - Home Depot PN: M550096
8. 1x ($7.83/each) ⅜-16 tap bit - McMaster-Carr PN: 2521A573
9. 1x ($24.94/each) ¼ NPT-18 tap bit McMaster-Carr PN: 2525A173
10. 1x ($9.58/each) T-handle tap wrench - McMaster-Carr PN: 25605A67
11. 1x ($1.21/each) 3/64-inch drill bit - McMaster-Carr PN: 8870A13
12. 1x ($3.68/each) 5/16-inch drill bit - McMaster-Carr PN: 8870A32
13. 1x ($7.32/each) 7/16-inch drill bit - McMaster-Carr PN: 8870A41
14. 1x ($29.97/each) Drill - Home Depot SKU: 1000052302
15. 1x ($19.08/each) ¾ inch hole punch - McMaster-Carr PN: 3424A51
16. 1x ($3.97/each) Scissors - Home Depot SKU: 1000042706
17. 1x ($10.94/each) ½ inch drive ratchet - Home Depot PN: 91-930
18. 1x ($2.49/each) 15/16-inch socket - Home Depot SKU: 631849

19. 1x ($7.97/each) Adjustable wrench - Home Depot SKU: 5386A3

20. 1x ($124.99/each) 8 gal 2 hp 125 psi air compressor - Harbor Freight PN: 68740

21. 1x ($18.42/each) Small gauge wire strippers - McMaster-Carr PN: 7294K15

Total (with air compressor): $203.35

Total (without air compressor): $328.34

Shock Tube Extension Sections

1. 1x (or more) ($18.28/each) 10 ft 3-inch schedule 40 PVC Home Depot (a 10 ft length makes 2 extension sections of 5 ft each)

2. 4x (for each 10 ft of PVC) ($16.32/each) 3-inch Schedule 80 PVC flange - McMaster-Carr PN: 4881K218

3. 2x (for each 10 ft of PVC) ($3.78/each) Gasket - McMaster-Carr PN: 1082N15

4. 2x ($3.04/each) Compression fitting - McMaster-Carr PN: 50915K315

Total: $97.20

Shock Tube End Section

1. 1x 5 ft 3-inch schedule 40 PVC (this is other half of 10 ft length used from high pressure (driver) assembly section)

2. 1x ($16.32/each) 3-inch schedule 80 PVC flange - McMaster-Carr PN: 4881K218

3. 1x ($3.78/each) Gasket - McMaster-Carr PN: 1082N15

4. 1x (option 1 for purchasing end wall) ($39.63/each) Blind flange McMaster-Carr PN: 6826K378

5. 1x (option 2 for purchasing end wall) ($5.65/each) spigot connector with cap - Home Depot SKU: 1001298506

6. 1x (option 2 for purchasing end wall) ($4.57/each) epoxy for filling cap - Home Depot SKU: 120618

Total: $59.73

Diaphragms

1. 1x Overhead sheets (box)
2. 1x Freezer paper (box)

Appendix C

Shock Tube Section CAD Drawings

Figure C1

CAD Rendering of Driver Section

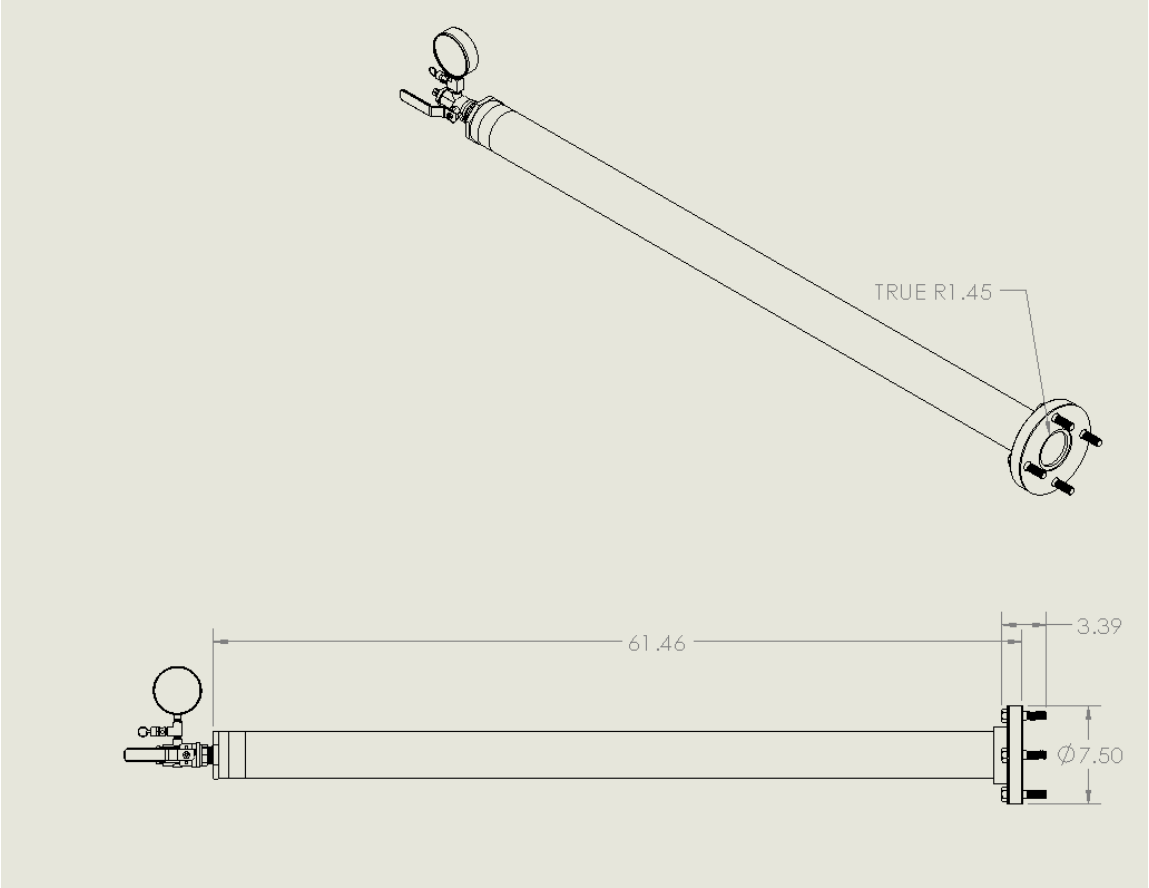

Figure C2

CAD Rendering of the Extension with Possible Porthole Locations

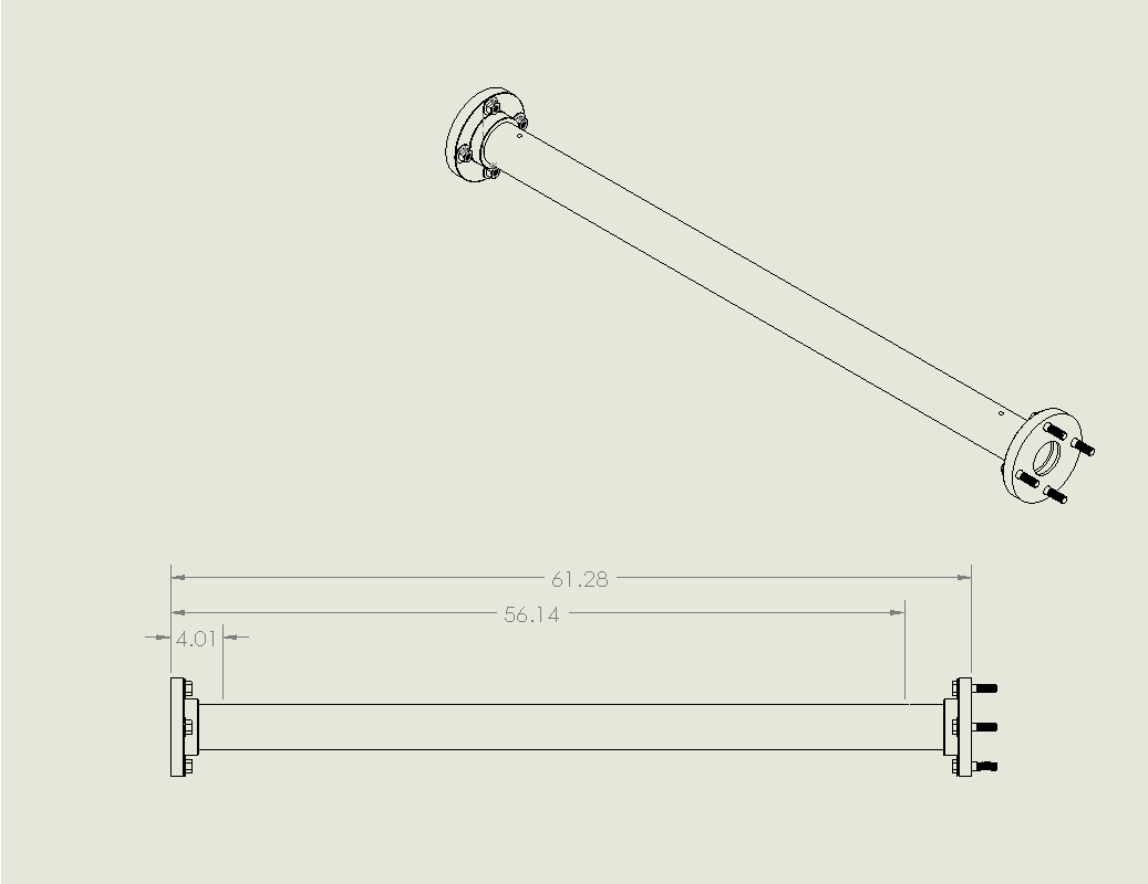

Figure C3

CAD Rendering of the End Section